Studies on Interaction Between Wind and Dry Snow Surface*

by

Shun'ichi KOBAYASHI
小 林 俊 一
The Institute of Low Temperature Science

Received December 1979

Abstract

Interaction between the wind and the surface of dry snow and bare ice has been studied by analyzing systematic and quantitative data obtained from field and laboratory researches on the formation of snow-waves, which represent one of a variety of deposition/erosion patterns (waves, ripples, barchans, sastrugi, dunes, pits, etc.) formed on a snowfield, as a wind redistributes a surface layer of deposited snow. Profiles of wind speed were obtained from measurements of wind speed in the lower surface layer, where snow drifts over dry snow and bare ice surfaces, in Hokkaido, Japan, and in Mizuho Plateau, East Antarctica, while parameters termed "roughness parameter" and "friction velocity" were calculated from both the surfaces to account for a drifting snow phenomenon to which the logarithmic wind profile law should be applicable.

Horizontal and vertical fluctuations of wind speed were obtained using sonic anemometers in the lower surface layer under a condition, in which transverse snow-waves are formed, i.e., the wind speed at the height of 1 m is more than 7 m s^{-1} after new snow accumulated to the thickness of 10 to 20 cm on a snow field. For example, when a snow-wave had a wavelength of 10 m and a wave height of 15 to 20 cm, the measured horizontal and vertical wind speed components showed that both of their coherence and cospectrum had a frequency peak of 0.7 Hz corresponding to this wavelength. The results suggest that wind turbulence and snow-wave formation are related with each other.

Turbulent fluctuations in the horizontal wind speed components were also obtained using sonic anemometers under a condition, in which snow drifting took place around the so-called "wind scoop", a snowdrift caused by an obstruction. A helicoidal stream around an obstruction (two small huts) was observed by trajectories of smoke and drifting snow particles. When a wind stream encountered an obstrucle or a surface irregularity, its boundary layer was separated and turbulent waves were formed around it. Accordingly, deposition and erosion were discussed in connection with local eddy patterns.

* Contribution No. 2184 from the Institute of Low Temperature Science.
北海道大学審査学位論文

Contents

I. Introduction

The surface stratum of air with a thickness of several tens of meters between the surface of the earth and the atmosphere provides the major place where energy is exchanged between the atmosphere and the surface of snow or ice. As the phenomenon of transportation of snow by the wind in the lower layers of this stratum constitutes a subject of special interest, fundamental studies have been made of it by a large number of investigators, including SHIOTANI and ARAI (1952), MELLOR and RADOK (1960), DYUNIN (1963), SOMMERFELD and BUSINGER (1965), BUSINGER (1965), BUDD et al. (1966), BUDD (1966), and Daiji KOBAYASHI (1972).

Despite that interactions between wind turbulence and snow have been well known by a study of CORNISH (1914) since about 60 years ago, our knowledge about the structure of wind turbulence over the surface of snow or ice during the drifting of snow is not so sufficient as to account for physcial processes controlling the way in which the wind and the surface of snow or ice interact with each other. Meanwhile, although there is a large literature on wind-waves and on theoretical work of flows over sand waves (e. g., BAGNOLD, 1954 ; KAWAMURA, 1951; TAYLOR and DYER, 1977; KENDALL, 1970), a theoretical treatment of snow-waves has not been made to date. Descriptions and classifications of surface reliefs formed by a wind action have, however, been made by many investigators, such as CORNISH (1914), HATAKEYAMA (1936), BAGNOLD (1954), DOUMANI (1966), ÔURA (1966) and KOBAYASHI (1971).

With the main purpose of identifying characteristics of interaction between wind turbulence and snow-wave formation, this paper presents new information about them, on the basis of studies carried out in Hokkaido in winter seasons and Mizuho Plateau, East Antarctica, from three aspects, i.e., characters of the mean wind speed profile during the drifting of snow, interaction between wind turbulence and the states of snow surface, and formation of a snow-drift around an obstruction.

II. Observational sites and measurements

Most of the observations were carried out in Sapporo, Japan, and in Mizuho Plateau, East Antarctica, the latter in 1973-74 during which the present author was a member of the 14th Japanese Antarctic Research Expedition. Table 1 shows a summary of surface and other conditions and air-snow interaction of the observational sites, in which among others, surface conditions varied with the site terms of density and hardness of snow.

Observations in Sapporo were conducted in the flat snowfield of Hokkaido University located in the north of the campus, extending about 400 m in the north-south distance. While the prevailing winds accompanied by drifting snow are mainly northwesterly, the depth of the snow cover is around 100 cm every years, with the surface density and hardness less than 0.3 g

Table 1. Summary of some case studies

Observation site	Climatic condition	Surface condition	Atmosphere condition	air-snow interaction
Hokkaido	Drifting snow	Soft snow (porous) $\rho<0.3$ g/cm^3 $H<0.2$kg/cm^2	neutral $R_i\approx 0$	surface features transfer phenomena
Antarctica	Katabatic wind region	hard snow $\rho\approx 0.3\sim 0.45$ $H\approx 1\sim 50$	stable $R_i\gtrsim 0$	heat budget (radiative cooling) transfer phenomena surface features gravity wave
		bare ice $\rho>0.85$ $H>500$	unstable (summer) $R_i\lesssim 0$	heat budget (ablation area) surface features hydraulic jump

cm^{-3} and 0.2 kg cm^{-2} respectively. Wind speed profiles were obtained using three-cup anemometers installed one each at five heights, for example, 2.00, 0.85, 0.35, 0.15 and 0.05 m. The wind turbulence near the snow surface during the drifting of snow was measured using a one-component ultrasonic anemometer manufactured by Kaijo Denki, Ltd. Electric signals from the anemometer were recorded by a one two-pen recorder on its paper chart. The sampling time ranged between 0.1 and 0.5 sec, and the recording time for each run between about 2 and 5 min.

Observations in Mizuho Plateau were made on a hard snow surface (surface density : 0.3~0.45 g cm^{-3}; hardness : 1~5 kg cm^{-2}) at a site of Mizuho Station (2230 m above sea level ; Lat. 70°42.0′S; Long. 44°18.9′E) and on a bare ice surface (surface density :>0.85 g cm^{-3} ; hardness :>500 kg cm^{-2}) at another site (1700 m above sea level ; Lat. 71°18′S ; Long. 35°40′E) near the Yamato Mountains. A map of the two observation sites in Antarctica is shown in Figure 1.

A series of micrometeorological and snow drift measurements were made on a katabatic wind slope (mean surface slope : 3×10^{-3}) at Mizuho Station in a period from April 15 to April 21, 1973, and a period from August 28 to September 23, 1973. Meteorological conditions at Mizuho Station are characterized by the blowing of stationary katabatic winds within the inversion layer over the surface slope (KOBAYASHI, 1977, 1978). The mean profile of wind speed was measured with five small anemometers of the three-cup type manufactured by Makino Instrument Company. The anemometers were installed on the tower one each at heights of 8, 4, 2, 1 and 0.35 m above the snow surface. The rotation of each anemometer was counted by a magnetic digital counter. The profile of temperature was observed by platinum resistance thermometers each with a shelter, which were set on the same tower one each at

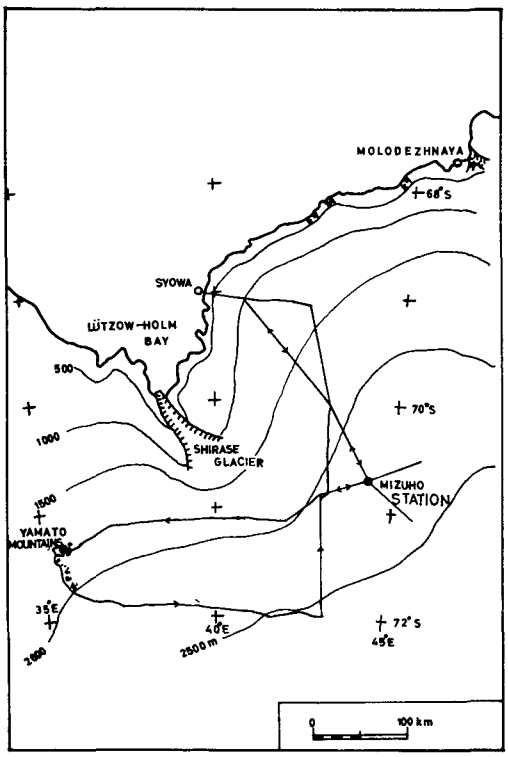

Fig. 1 Map showing two observation sites, Mizuho Station and the Yamato Mountains.

heights of 4, 2, 1 and 0.5 m above the snow surface. The outputs of the thermometers were automatically recorded every minute by a six-channel recorder. Fluctuating wind velocity components and air temperatures were measured simultaneously by a three-dimensional ultrasonic anemometer-thermometer (called S.A.T. hereafter), which was mounted at the height of 4.5 m.

Electric signals from the S.A.T. were recorded on the four-channel rectigraph 40 mm in width (per one channel) with a chart speed of 50 mm/sec. The response time of the recorder was about 0.03 sec. The sampling interval was between 0.1 and 0.2 sec, and the recording time for each run was about 5 min.

Meanwhile, micrometeorological observations were carried out on the bare ice field near the northern Yamato Mountains from December 1 to 7, 1973. The observation site, as shown in Figure 2, is located on the leeward of massifs E and F of the Yamato Mountains. The prevailing wind near the surface was almost easterly. This is an area marked by the occurrence of a hydraulic jump due to a strong turbulence which is generated by nunataks. Five three-cup anemometers were installed one each at the heights of 3.35, 1.85, 0.86, 0.55 and 0.35 m. Air temperatures were measured using thermister thermometers installed one each at the heights of 3.15, 1.65 and 0.15 m. Observations were made of wind turbulence using a one-component ultrasonic anemometer, which was mounted at the height of 2.2 m. Electric signals from the sonic anemometers were recorded by a one-pen recorder on its paper chart. The sampling time was 0.83 sec and the recording time for each run was about 10 min.

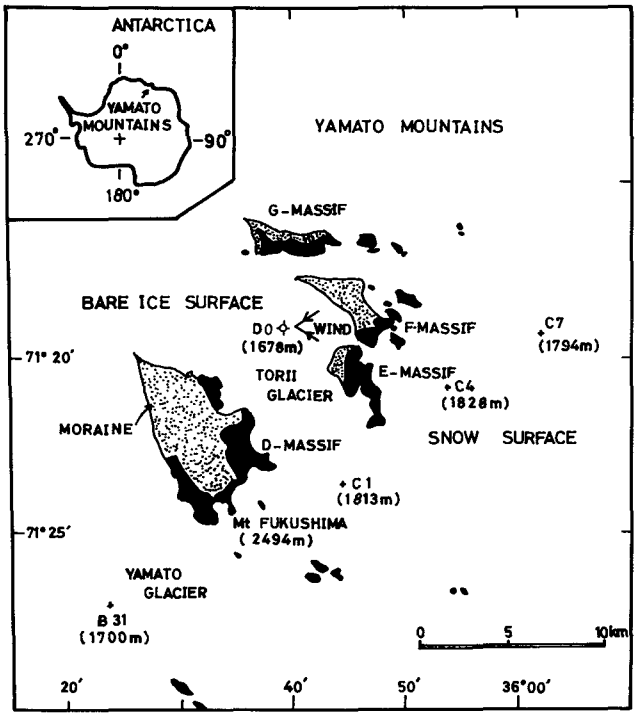

Fig. 2 Location map of observation site (DO) near the northern Yamato Mountains.

III. Surface features of flat snow surfaces

III. 1. *Classification of deposition/erosion patterns*

For description of interaction between wind and snow a study was made of features of a flat snow surface. As a wind redistributes a surface layer of deposited snow, surface microreliefs are formed on a snowfield, as shown in Figures 3~8. Their general characteristics and dimensions are known, while their modes of formation are understood in broad terms (e.g. MELLOR, 1965). But there is little systematic and quantitative information on details of the formation.

Microreliefs formed during the drifting of snow can be classified according to deposition/erosion patterns; i.e., sastrugi (Figure 3) and pits (Figure 4) are formed when erosion is dominant, whereas ripples (Figure 5), dunes (Figure 6), barchans (Figure 7), are waves (Figure 8) are formed when deposition is dominant. Another classification divides microreliefs into transverse features (ripples, waves, barchans) and longitudinal features (dunes, sastrugi, pits). In

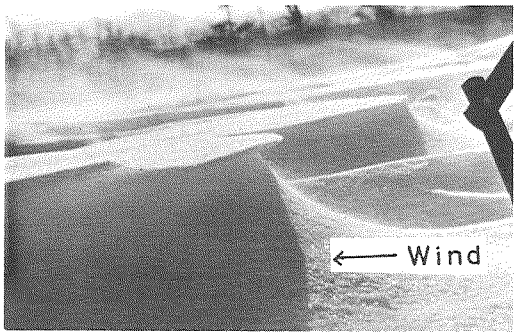

Fig. 3 Photograph of sastrugi in Sapporo.

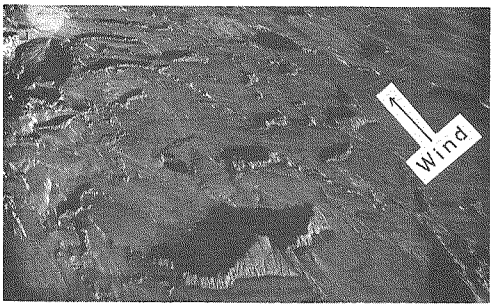

Fig. 4 Photograph of pits in Antarctica.

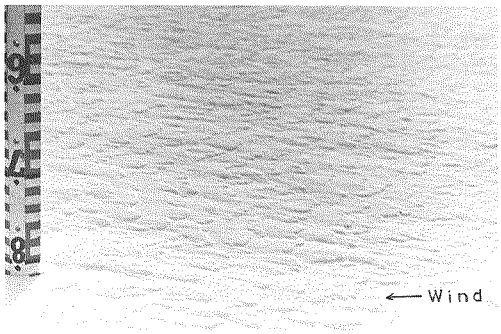

Fig. 5 Photograph of ripples in Sapporo.

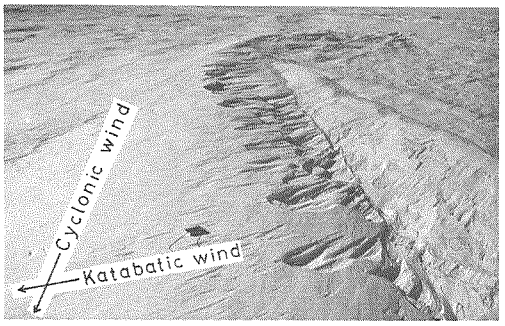

Fig. 6 Photograph of a dune in Antarctica, its direction coinciding with the direction of the cyclonic of the cyclonic wind and the erosional patterns above it having been formed by a katabatic wind.

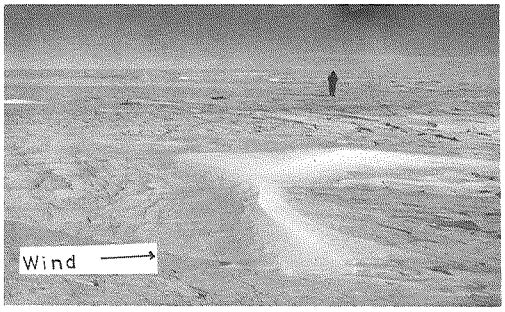

Fig. 7 Photograph of a snow barchan in Antarctica.

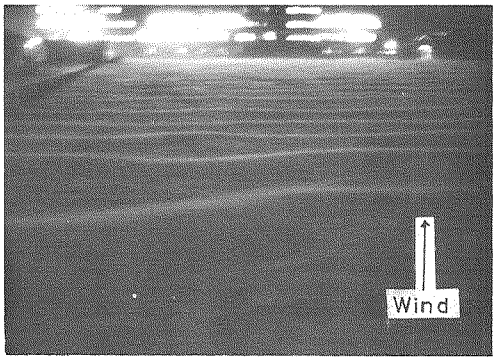

Fig. 8 Photograph of snow-waves in Sapporo.

general, the former are formed by light winds, whereas the latter are formed by strong winds (MELLOR, 1966).

III. 2. *General characteristics of sastrugi and pits*

Sastrugi and pits, as shown respectively in Figures 3 and 4, were formed when the snow surface was eroded, their alignment being in the direction of the wind. Pits moved at the speed of less than 1.0 cm min^{-1} during their formation period. Some of the pits were transformed into sastrugi, depending on wind speed. The movement of sastrugi was observed by slow motion pictures taken by a 16-mm movie camera and still photographs taken by a 35 mm camera. The movement speed obtained by the above method ranged from 0 to 1.0 cm min^{-1}, as shown in Figures 9 and 10. Although they were caused by wind erosion, sastrugi ceased to move after age hardening had made the snow surface stable.

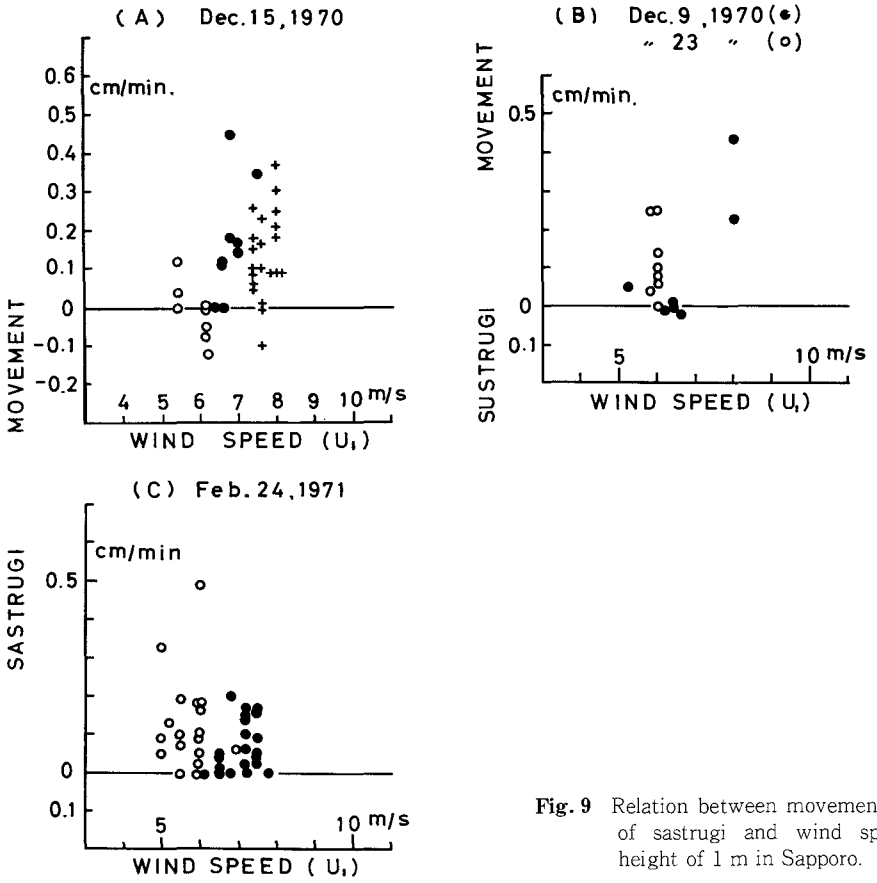

Fig. 9 Relation between movement speed of sastrugi and wind speed at height of 1 m in Sapporo.

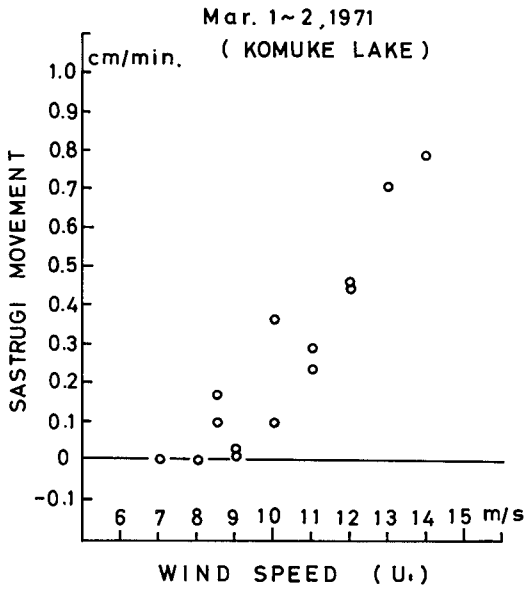

Fig. 10 Relation between movement speed of sastrugi and wind speed at height of 1 m measured at Lake Komuke in northern Hokkaido.

III. 3. *General characteristics of ripples*

Ripples, as shown in Figure 5 are small transverse waves 5 to 10 cm in wavelength and 2 to 5 mm in wave heigh (from the trough to the crest). Formed at a time when and a place where deposition was dominant, they were transformed into sastrugi (longitudinal features) as the wind speed increased. Ripples moved at the speed of less than 0.5 cm min^{-1}. It is easy to demonstrate the formation of ripples, as seen at night when snow is depositing on a lighted table, which is buried under a snow surface, as shown in Figure 11. A photograph of ripples taken by the above method is shown in Figure 12.

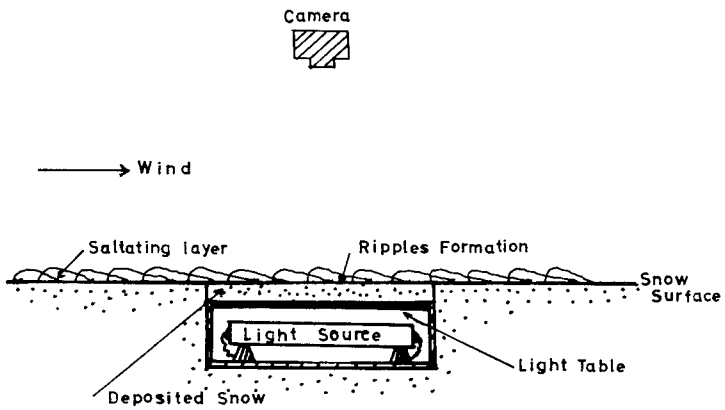

Fig. 11 Illustration of a lighted table buried at depth of 1 cm below the snow surface for observation of formation of ripples at night.

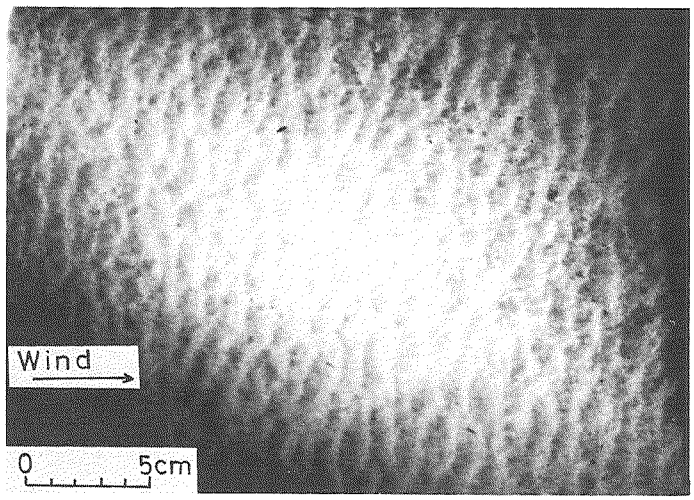

Fig. 12 Formation of ripples seen on a lighted table. When developed, ripples have a wavelength of about 1 cm.

III. 4. *General characteristics of dunes*

Dunes, as shown in Figure 6, which are also called wholeback dunes, as associated with strong winds blowing during the passage of a cyclonic snowstorm (blizzard) in Antarctica, at which time much new snow is deposited on the ice sheet. Dunes are aligned in the longitudinal direction. In Antarctica, sastrugi and pits are etched on dunes in differential angles to the direction of dunes, as seen in Figure 6. They prove the presence of two winds systems in Antarctica, i.e. katabatic and cyclonic winds (ÔURA and YAMADA, 1966; AGETA, 1971; WATANABE, 1978). It is difficult to see the formation of dunes in such an Antarctic blizzard as is under severe conditions.

III. 5. *General characteristics of barchans*

A barchan, as shown in Figure 7, is usually formed, as previously deposited snow is redistributed by a "dry" wind like a katabatic wind in Antarctica. Also, a barchan is formed on a mountain slope as shown in a photograph of Figure 13. Measurements conducted in Antarctica disclosed that a barchan moved at the speed of 3 cm min^{-1} when wind speed at the height of 1 m was 11 m sec^{-1}. Movement of a barchan is

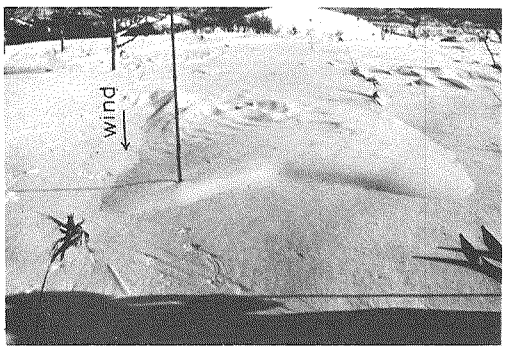

Fig. 13 Photograph of a barchan formed on a mountain slope in Hokkaido.

the same as that of a transverse snow-wave, i.e. a drift.

III. 6. *General characteristics of transverse snow-waves*

The term "wave" has been applied to a transverse undulation which has the appearance of a sea wave. Snow-waves, as shown in Figure 8, were formed when a wind blew at the speed of more than 7 m sec^{-1} at the height of 1 m after snow had accumulated to more than 10 cm in thickness on a snowfield. Although snow-waves are classified as a deposition type, deposition and erosion occur generally in an alternating sequence. Whether the snow surface had been eroded or deposited was determined experimentally by measuring a change in snow surface level by a scaled stake. An example of the measured results is shown in Figure 14, in which the snow surface level fluctuates. In the figure, period (1) shows a time sequence during active formation of waves, whereas period (2) shows a time sequence when wave formation was weakened despite that snow was blowing, whereas period (2) is marked by stabilization of the snow surface, because the income and the outgo of snow particles are balanced in this snow-field.

Movement of snow-waves was also observed by slow motion pictures taken by a 16-mm movie camera. An example of a wave travel is shown in Figure 15, a case in which the travel speed is about 4.3 cm min^{-1}. A relation between the travel speed of a snow-wave and the wind speed at the height of 1 m was obtained in the snowfield of the campus of Hokkaido University. The travel speed ranged from 2 to 10 cm min^{-1}, as shown in Figure 16. These values are larger than those of sastrugi which move at the speed less than 1 cm min^{-1}, as shown in the same figure. The snow-waves had wavelenths from 3 to 15 m and wave heights from 5 to 20 cm.

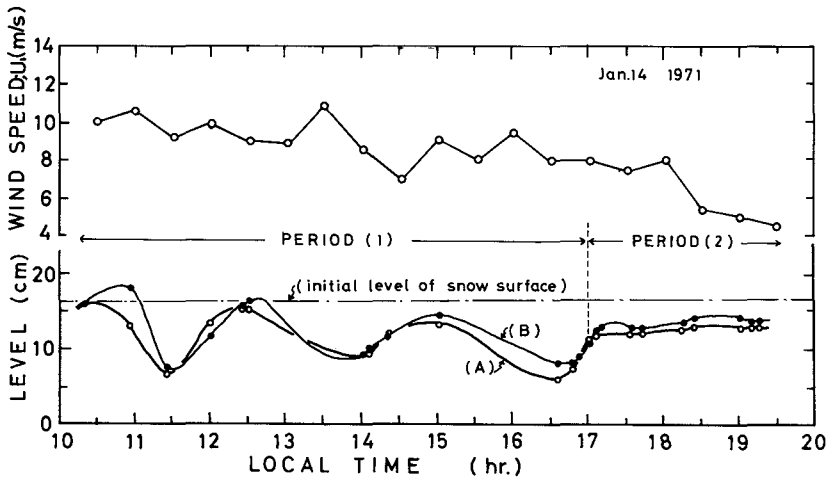

Fig. 14 Change in snow surface level with lapse of time. Period (1) : active wave formation; period (2) : stable surface. Stake (A) is located 1 m windward from stake (B). This wavy surface has a wavelength of 5 m.

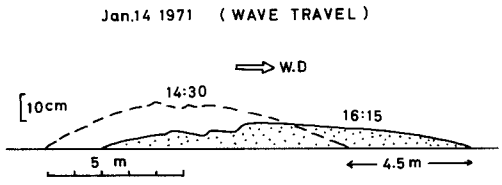

Fig. 15 Example of wave travel. Travel speed : 4.3 cm min^{-1}

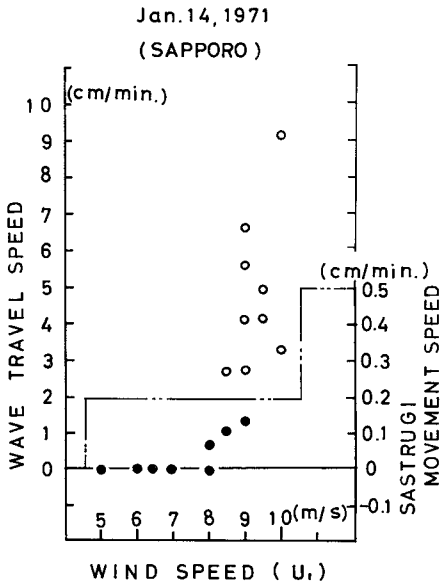

Fig. 16 Relation between travel speed of a snow-wave and wind speed at height of 1 m. Open and solid circles represent snow-waves and sastrugi, respectively.

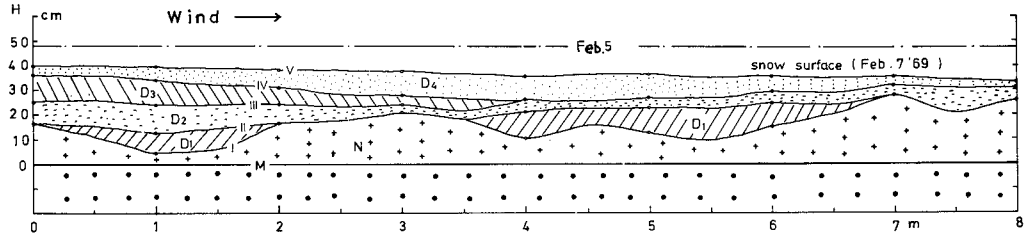

Fig. 17 Stratigraphic structure of a pit wall of a long trench 8 m in length along a prevaliling wind direction observed in Sapporo. Before a snowdrift started, the new snowcover had the thickness of 48 cm corresponding to the level of surface on Feb. 5, when it ceased, the level of the surface showed the mark V.

Eroded patterns like sastrugi were formed in wave troughs. These may be related to the phenomenon known as separated flows.

As is described later, the wavelegth of a snow-wave vaires inversely with the mean wind speed. In particular, the wavelength approaches zero when the mean wind speed at the height of 1 m rises above 15 m sec^{-1}. This means that a transverse feature will disappear in a strong wind, because of the predominance of longitudinal characteristics of the wind. In general, after snowdrift formation, we can rarely see snow-waves on the snowfield, because the surface

gradually becomes flat. For instance, after a snowdrift has been formed, observations can be made of areal variations. The stratigraphic structure of the pit wall of a long trench about 8 m in length along a prevailing wind direction has been studied. The result is shown in Figure 17. The analysis showed that the stratification was caused by alternating erosion and deposition in each portion of the long pit wall and that, when snow drifting period came to an end, the snow surface became flat. It is of special interest that a past history is preserved in the snow layer.

Ⅳ. Charcteristics of parmeters of mean surface wind profile

Ⅳ. 1. *Wind profiles above flat surfaces of snow and bare ice*

As is known well, when the wind is strong and the air mass above a flat snowfield showes neutral stratification, the following logarithmic relationship holds between wind speed U_z and height above surface Z, at least in the lower layers in which blowing snow occurs :

$$U_z=(U_*/K)\cdot 1n(Z/Z_0), \tag{1}$$

where U_* is the "friction velocity" defined by $(\tau_0/\rho)^{\frac{1}{2}}$ (τ_0 : the surface shear stress ; ρ : the air density), k the numerical constant (von Karman's constant) equal to 0.4, and Z_0 the roughness parameter, a length generally considered as characterizing the surface. When field measurements of U are plotted against log Z, the intercept and slope give Z_0 and U_* respectively.

Examples of wind profiles obtained in a snowfield on the campus during the drifting or nondrifting of snow are given in Figure 18. Air temperature profiles showed a nearly neutral condition over all the observational period. Meanwhile, typical wind profiles obtained at Mizuho Station under the weak stable stratification showed that the wind speed increased with an increase in height, deviating from a logarithmic straight line, as shown in Figure 19(a). Also air temperature profiles corresponding to wind profiles of Figure 19(a) are shown in Figure 19(b). However, the logarithmic relation of a wind profile has been found to hold in the lower layer less than 2 m above the snow surface, where buoyancy forces may be neglected. Wind profiles and air temperature profiles

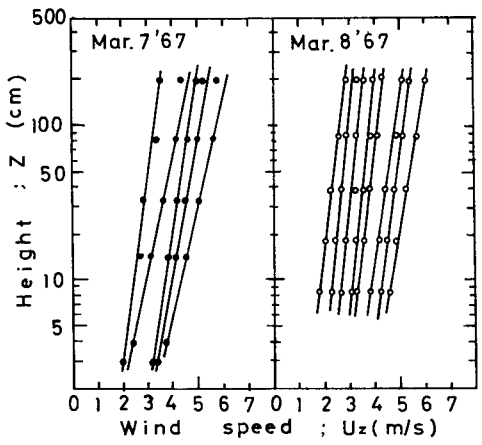

Fig. 18 Examples of wind speed profiles measured is Sapporo. March 7: drifting snow : March 8 : nondrifting snow.

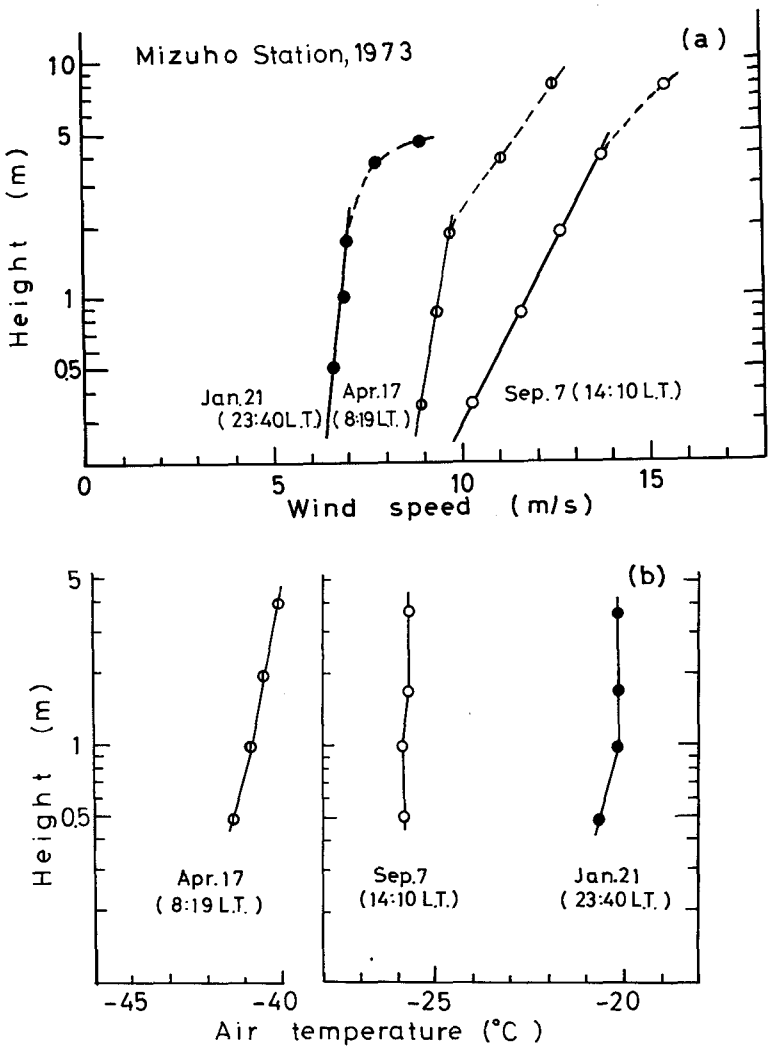

Fig. 19(a). Examples of wind speed profiles measured at Mizuho Station.

Fig. 19(b). Exapples of air temperature profiles measured at Mizuho Station. Each profile corresponds to the profile of wind speed dated the same in Fig. 19(a).

above the bare ice surface were obtained in the Yamato bare ice field, as shown in Figure 20(a) and (b), respectively. Although the atmosphere showed unstable stratification, wind profiles showed logarithmic straight lines at the height less than 4 m. Since energy production and energy dissipation balance most near the surface, the logarithmic law may be applicable.

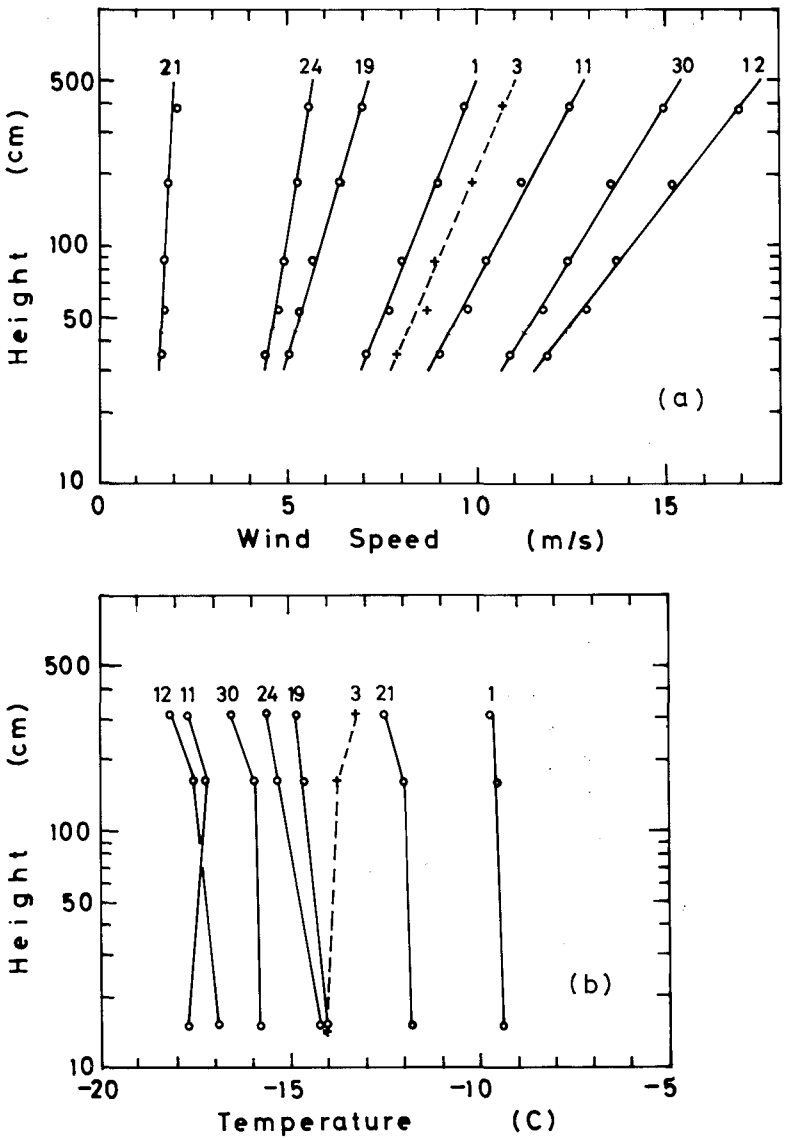

Fig. 20(a). Examples of wind speed profiles measured in the Yamato bare ice field.

Fig. 20(b). Examples of air temperature profiles measured in the Yamato bare ice field. Each run numbered corresponds to the profiles of wind speed numbered the same in Fig. 20(a).

IV. 2. *Variations in roughness parameter above surfaces of soft snow, hard snow and bare ice*

The roughness parameter is important in the calculation of fluxes of momentum and matter in the surface layer. As described in the above section, the roughness parameters Z_0 for the snow or ice surface are frequently reported by many investigators, such as LILJEQUIST (1957), UNTERSTEINER and BADGLEY (1965), BUDD et al. (1966), ÔURA et al. (1967), HOLMGREN (1971), MAKI (1972), KIKUCHI and ISHIDA (1976), and JACKSON and CARROLL (1978). Figure 21 shows the values of Z_0 plotted against friction velocity U_* (as described in next section corresponding to the wind speed) during the drifting and nondrifting of snow, obtained in the snowfield of Hokkaido University. The values of Z_0 scatter over roughly three orders of magnitude in a period of drifting snow, from 0.001 to 0.1 cm, and in a period of nondrifting snow, from 0.0001 to 0.01 cm. The typical surface textures were ripples or small sastrugi. However, the values of Z_0 increase with increasing wind speed in all cases. KIKUCHI and ISHIDA (1976) reported that an increase in roughness paramenter during the drifting of snow supported Bagnold's empirical relation (1954) instead of the relation $Z_0 \propto U_*^2$.

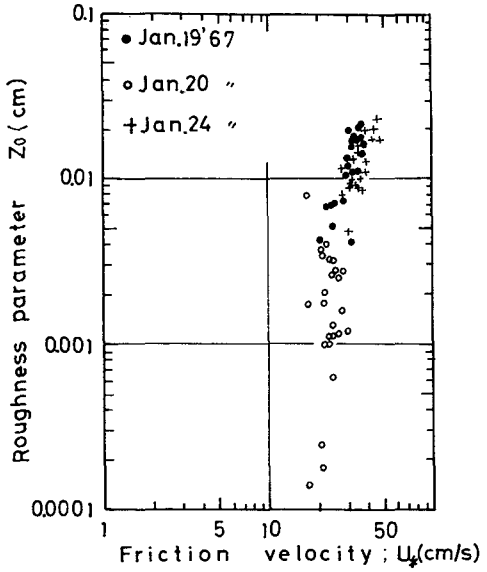

Fig. 21 Relation between roughness parameter and friction velocity measured in Sapporo. Marks (●) and (+) show plots of drifting snow, and (○) plots of nondrifting snow.

On the other hand, the values of Z_0 measured at Mizuho Station might be related to the hard snow surface, as compared with the surface in Sapporo. Roughness parameters were obtained at Mizuho Station during the austral spring and winter of 1973. Figures 22 and 23 show the resulting values of Z_0 plotted against friction velocity and wind speed at the height of 1 m, respectively. The values of Z_0 shown in Figure 22 varied with the wind speed, having the mean value of 0.015 cm and ranging from 0.002 to 0.4 cm. Figure 23 shows that the values of Z_0 scatter over the roughly four orders of magnitude, from 0.00001 cm to 0.03 cm. The most conspicuous feature is a marked increase in Z_0 with decreasing wind speed. This variation in Z_0 has been found in case of light to moderate winds, but in case of strong winds the variation in Z_0 indicated an increase in surface roughness with increasing wind speed at some other stations such as Maudheim (LILJEQUIST, 1975), Mirny (RUSIN, 1961), Byrd (BUDD et al., 1966) in Antarctica and Ice Cap on Devon Island in Arctic (HOLMGREN, 1971). The typical surface texture in the vicinity of Mizuho Station is produced by wind erosion which creates sastrugi.

Sastrugi are aligned with their major axes parallel to the direction of the generating wind, i.e. katabatic wind. Uniformly distributed, they rarely exceed 50 cm in height. According to NIKURADSE's result (e.g. MONIN and YAGOLOM, 1971), Z_0 is equal to about 1/30 of the height of actual roughness elements of the surface. Using the maximum value of 0.4 cm, the above relationship shows that the height of actual sastrugi corresponds to 12 cm. But in parctice it is difficult or impossible to identify sastrugi. The influence of atmosphere stability on the roughness parameter may be discussed as follows : Mizuho Station is located on a katabatic wind slope. The katabatic wind in Antarctica represents the downward movement of an air mass, which has been cooled as the result of the radiating cooling of the ice sheet at its surface, along the slope by gravity, so the layer of the katabatic wind is roughly identical with the surface inversion layer. The annual mean speed of katabatic winds at Mizuho Station is as high as 10~11 m sec^{-1}. Therefore, when the wind is light or moderate, a surface inversion can develop above to ice sheet, so the wind speed increases under a stable condition of the atmosphere. Then, pure drifting snow occurs when the sky is clear. On the other hand, a surface inversion layer is can be destroyed by a strong wind caused by a cyclone passing over the ocean in the vicinity of Syowa Station and drifting snow occurs under a condition in which snow falls. Then the surface roughness can increase with an increase in wind speed.

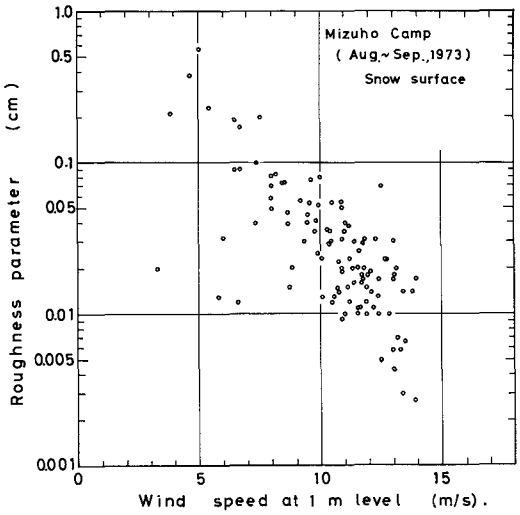

Fig. 22. Relation between roughness parameter and wind speed at height of 1 m obtained in austral fall at Mizuho Station.

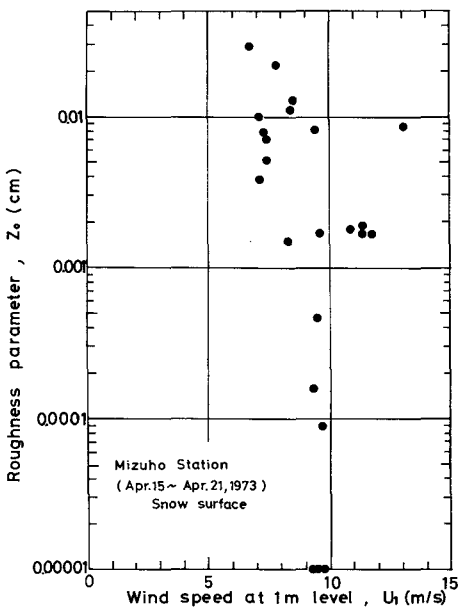

Fig. 23 Relation between roughness parameter and wind speed at height of 1 m obtained in austral winter at Mizuho Station.

Finally, a relation between Z_0 and wind speed at the height of 1 m was obtained in the Yamato bare ice field, as shown in Figure 24. The value of Z_0 was constantly 0.087 cm independent of the wind speed. The surface of a bare ice surface at the observation site had a spoon-cut feature 2~3 cm in depth, as shown in Figure 25. If Z_0 is equal to about 1/30 of the height of actual roughness elements, then the calculated value is 2.6 cm corresponding to the depth of spoon-cut features on the bare ice surface.

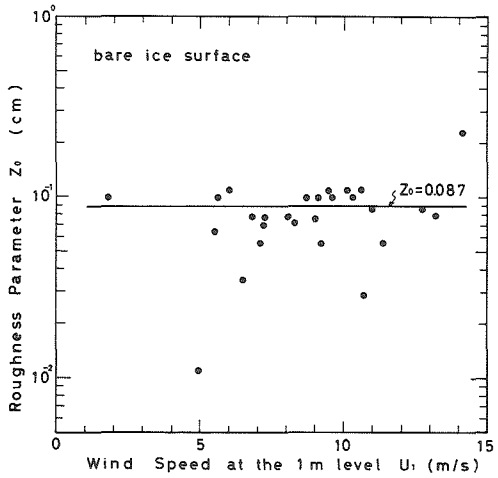

Fig. 24 Relation between roughness parameter Z_0 and wind speed U_1 at height of 1 m obtained in the Yamato bare ice field.

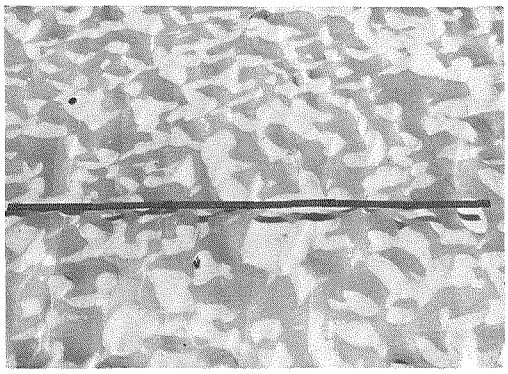

Fig. 25 Surface feature of a bare ice surface near the northern Yamato Mountains. Scale : 1 m.

IV. 3. *Relation between friction velocity and wind speed*

The atmosphere is viscous, which means that the surface exerts a fricitional drag; hence, the wind speed near the surface increases with height. The force of retardation per unit surface area is known as the surface shearing stress τ_0 in units of dynes cm^{-2}. This shearing stress originates at the surface, but exists through the surface boundary layer. The surface layer is also defined as a "constant flux layer" with the constant value of τ_0. Wind shear is known by a change in wind speed with height. As described before, the quantity $(\tau_0/\rho)^{\frac{1}{2}}$ has the dimension of velocity and it is convenient to define the friction velocity U_*. The friction velocity is proportional to the inclination of a wind speed profile in the diagram of log-height versus wind speed. The shearing stress per square centimeter of a snow surface in Sapporo is derived from U_* by the equation $\tau_0=\rho U_*^2$. The relation between τ_0 and U_1, which is the wind speed at the height of 1 m, is shown in Figure 26. In the figure, solid circles and cross marks for drifting snow are represented by the lines $\tau_0 \propto U_2^{2.6}$ and white circles for nondrifting snow by the lines $\tau_0 \propto U_1^{1.5}$. The magnitude of shearing stress depends upon wind speed, whether or not snow is drifting, surface roughness and surface condition. In term of the surface condition, values of

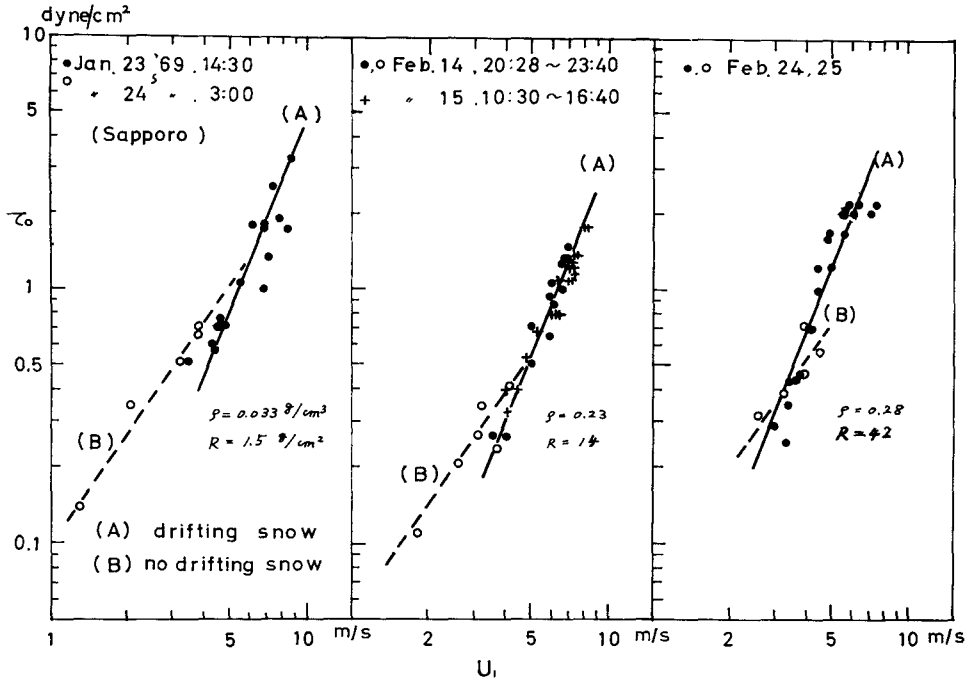

Fig. 26 Relation between shear stress (τ_0) and wind speed at height of 1 m. Solid lines (A) : equation $\tau_0 \propto U_1^{2.6}$ ($U_* \propto U_1^{1.5}$) for drifting snow ; dashed line (B) : equation $\tau_0 \propto U_1^{1.5}$ ($U_* \propto U_1^{0.7}$) for nondrifting snow.

surface snow density and hardness during measuring periods are shown in the figure.

Variations in friction velocity with wind speed at the height of 1 m were obtained at Mizuho Station in austral spring and winter, 1973, as shown in Figures 27 and 28. If we take a constant value for Z_0 as the mean value, then the friction velocity varies linearly with the wind speed at a given height, as derived from equation (1). In particular, if U_1 is the wind speed at the height of 1 m, then in Figure 27

$$U_*=0.038U_1, \text{ for } Z_0=0.003 \text{ cm}, \quad (2)$$

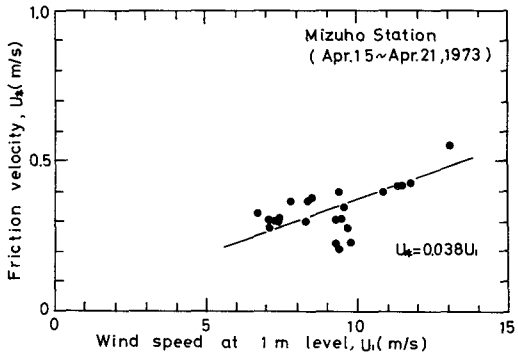

Fig. 27 Relation between friction velocity and wind speed at height of 1 m obtained in austral spring at Mizuho Station. A solid line $U_*=0.038U_1$ was calculated from equation (1) when $Z_0=0.003$ cm.

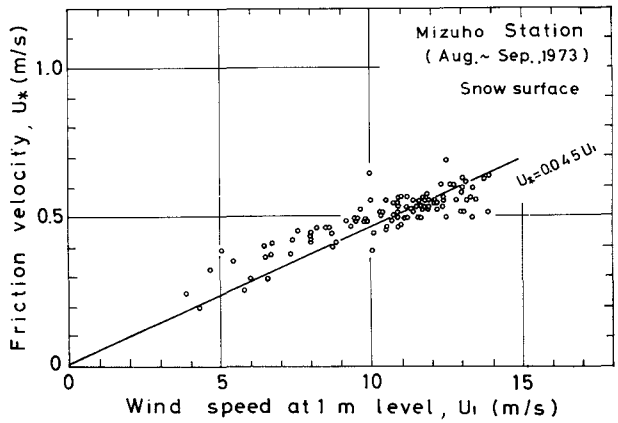

Fig. 28 Relation between friction velocity and wind speed at height of 1 m obtained in austral winter at Mizuho Station. A solid line $U_*=0.045U_1$ was calculated from equation (1) when $Z_0=0.015$ cm.

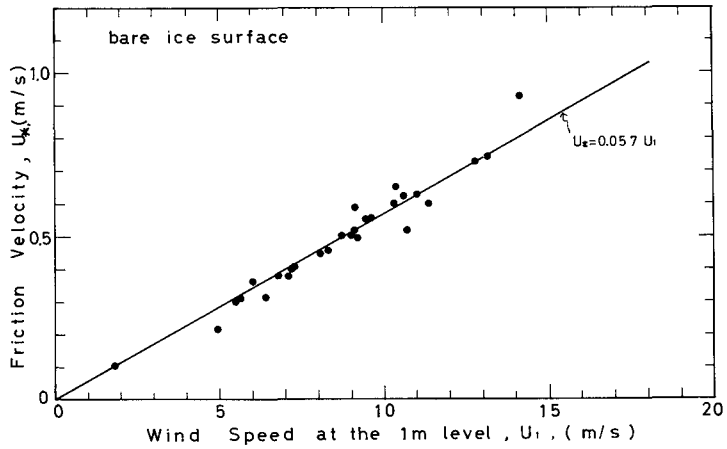

Fig. 29 Relation between friction velocity and wind speed at height of 1 m obtained in the Yamato bare ice field. A solid line $U_*=0.057U_1$ was calculated from equation (1) when $Z_0=0.087$ cm, which holds constantly, as shown in Fig. 24.

and in Figure 28

$$U_*=0.045\ U_1, \text{ for } \bar{Z}_0=0.015 \text{ cm.} \tag{3}$$

Therefore, the surface was aerodynamically smoother in spring than in winter. Figure 29 shows the friction velocity obtained on a bare ice surface near the Yamato Mountains. Since the value of Z_0 was constantly 0.087 cm independent of wind speed, the relation between friction velocity and wind speed at the height of 1 m is expressed by equation (4),

$$U_*=0.057U_1, \text{ for } \bar{Z}_0=0.087 \text{ cm.} \tag{4}$$

IV. 4. Relation between surface snow density and threshold shear stress

Knowledge of the wind drag force (or shearing stress) is of basic importance to studies of mechanisms of generation of drifting snow. ÔURA et al. (1967) discussed a relation between temperature and the generation of drifting snow in both field observations and wind-tunnel tests. They pointed out that the threshold wind speed necessary for the occurrence of drifting snow decreased with decreasing temperature for a temperature range 0 to about −7°C and showed the constant wind speed of about 6.5 m sec^{-1} for a temperature range from 0 about −7 to −23°C or much lower degrees. A theoretical explanation of this relation was attemped by ÔURA (1968). Meanwhile, finding that the amount of snow drift transport increased as temperature decreased, NARITA (1978) pointed out that snow drifting is controlled not only by wind speed but also by snow surface condition (soft or hard), particle shape of snow, and air temperature.

Thought it is difficult to estimate the value of threshold shear stress necessary for the occurrence of drifting snow, an approach to it may be provided by Figure 26. It suggests the value of τ_0, which corresponds to a point of intersection of two lines, i.e. a line for drifting snow and a line for nondrifting snow. This value of τ_0 means a threshold shear stress for generation drifting snow under saltation motion. Daiji KOBAYASHI (1972) showed that drifting snow near the snow surface is transported mainly by saltating motion, as evidenced by photographs of this motion he took. The result from Figure 26 suggests a relation between surface snow density and threshold shear stress, as shown in Figure 30.

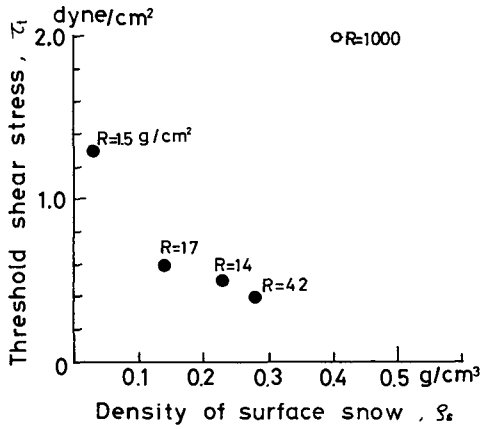

Fig. 30 Threshold shear stress for generation of drifting snow against density of snow surface. R: value of surface hardness ; solid cricle : obtained in Sapporo, blank circle : obtained in Antarctica.

According to eye measurements by YAMADA (1974) of frequencies of occurrence of drifting snow, the threshold wind speed was 5 m sec^{-1} at the height of 1 m in Antarctica. Using Figure 28 and a white circle plotted in Figure 30, a threshold friction velocity was obtained, which 0.4 m sec^{-1} corresponding to the value of 2 dyne cm^{-2}. Figure 30 shows that the threshold shear stress decreased with increasing density of surface snow up to 0.3 g cm^{-3}. If the density of surface snow becomes larger than 0.4 g cm^{-3}, however, then the threshold shear stress tends to increase with increasing density of surface snow.

From the saltation theory for sand, BAGNOLD (1954) derived an equation for the threshold friction velocity U_{*t} of the from ;

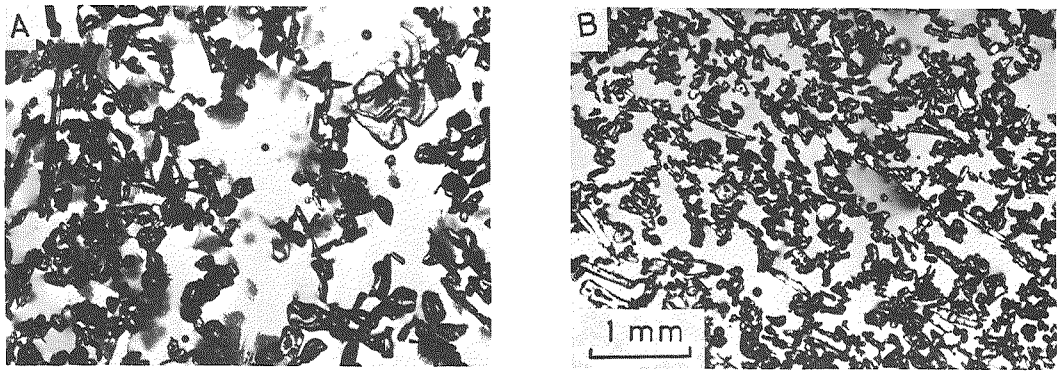

Fig. 31 Photographs of thin sections of snow (density : 0.24 g cm^{-3}; hardness : 150 g cm^{-2}). prepared by the anilin method. (A) : from eroded surface ; (B) : from depositional surface.

$$U_{*t}=A\left\{\left(\frac{\sigma-\rho_a}{\rho}\right)gd\right\}^{\frac{1}{2}}, \tag{5}$$

where ρ_a is the fluid density, σ the particle density, d the particle diameter, g the accelaration due to gravity and A the dimensionless quantity. Equation (5) shows that the threshold friction velocity increases with increasing diameter of a particle. Figure 31 shows two photographs of thin section prepared by the aniline method (KINOSITA and WAKAHAMA, 1956), the one (A) sampled from an eroded part and the other (B) from depositional part in a surface layer. Although the shapes of snow particles are complex, as shown in the two photographs, it is found that in the eroded part larger falling particles remain, whereas in the depositional part smaller particles stay on the surface. This result supports equation (5). Therefore, since the complexity of new deposited snow particles may correspond to the larger particles, the threshold shear stress in smaller density of snow than 0.1 g cm^{-3} tends to increase.

V. Wind-tunnel experiments on generation of drifting snow and wind structure near the surface

V. 1. *Instruments and methods*

As mentioned in the above section IV. 4. studies of mechanisms of generation of drifting snow call for knowledge on the drag force exerted on the snow surface by the wind. Thus, the drag force was directly measured, and the values obtained were compared with the values of drag force obtained by the wind profile method, by measuring the vertical distribution of wind speed above the snow surface by use of a sensitive hot wire anemometer in a wind-tunnel set in a cold room. The working part of the wind-tunnel, which is shown in Figure 32, is 30×30 cm

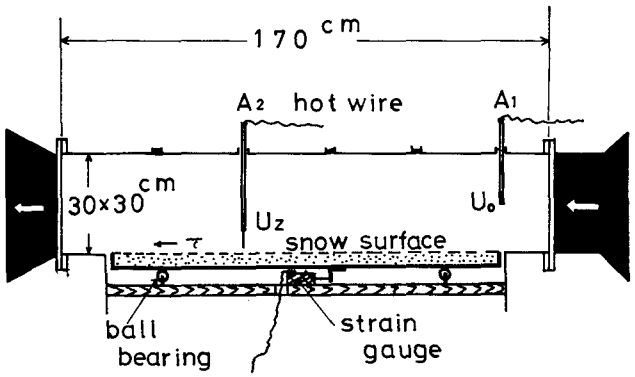

Fig. 32 Working part of a wind tunnel. Dimensions in cm. Arrows show wind direction. A_1: hot-wire anemometer measuring wind speed at center of the tunnel; A_2: sensitive hot-wire anemometer measuring wind speed profiles near the surface.

in cross section and 170 cm in length. The sides and top of the working part are made of transparent plates of acrylic acid resin 2 cm in thickness. Newly fallen snow particles were collected from the field and sieved in a shallow container made of aluminum 135×28×2 cm in size. The apparent snow density was 0.3 g cm^{-3}. This container filled with the snow was sustained with frictionless steel ball bearings in a wind-tunnel. A sensitive strain gauge (±200 g) was used to measure the drag force. The vertical distribution of wind speed above the snow surface was obtained by use of a sensitive hot wire anemometer, which is equipped with a very small tip with a thin hot wire made of tungsten 5 μ in diameter and 1 mm in length. This insturment was also used for the simultaneous measurements of intensity of turblence.

V. 2. *Wind drag force on the surface by wind*

When the flow velocity of air in the tunnel was raised, the drag force acting on the snow surface increased, as shown in Figure 33. In this case, when the wind speed measured at the center of the tunnel was raised to 12 m sec^{-1}, snow particles began to be ejected from the surface, but continuous ejection did not occur until the wind speed exceeded 17 m sec^{-1}, which

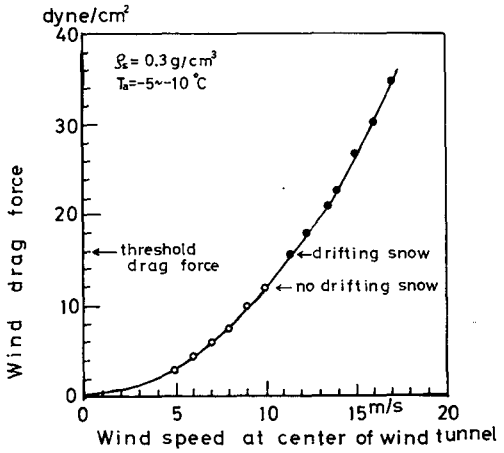

Fig. 33 Relation between wind drag force and wind speed at center of the wind tunnel. ρ_s: snow density; T_a: room temperature.

corresponds to the drag force of 35 dyne cm^{-2}, corresponding to 17 m sec^{-1} i.e. the friction velocity $U_*=164$ cm sec^{-1}. Beyond this wind speed, the snow particles were steadily ejected from the entire area of the snow surface. As known from Figure 30, the threshold drag force was smaller than 2 dyne cm^{-2} in nature. Accordingly, consideration should be given to the discrepancy in value of threshold drag force between the wind-tunnel and nature. The discrepancy suggests that the ejection of snow particles from the snow surface by wind action may hardly occur in nature, i.e., the generation of drifting snow in nature is explained by the mechanical impingment of a snow particle saltating on the snow surface. The saltation of snow particles on the snow surface was photographed by Daiji KOBAYASHI (1972). Meanwhile, other hand, KUROIWA (1975) calculated the velocity of a saltating snow particle which was required to break a sintered neck, assuming that the kinetic energy of the saltating particle is

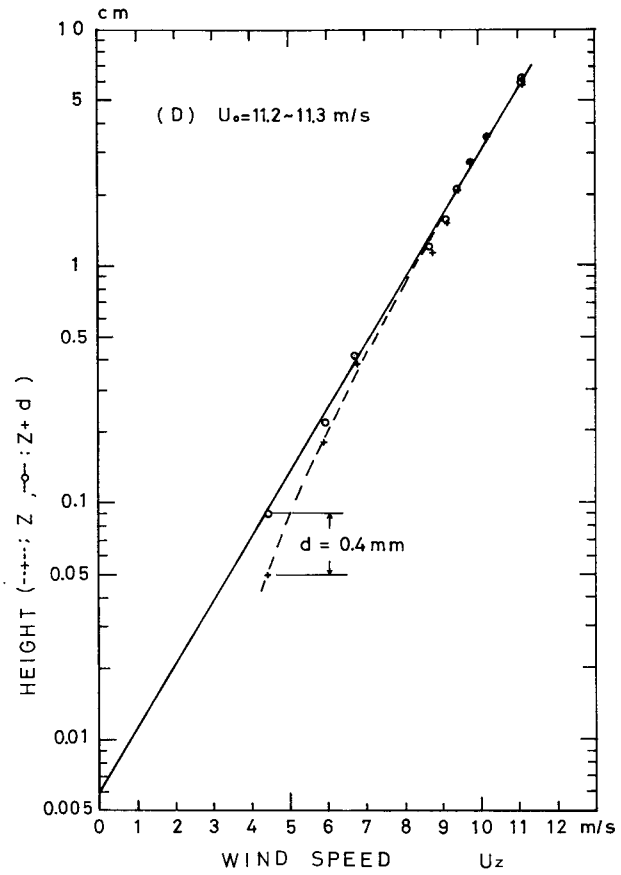

Fig. 34 Example of vertical distribution of wind speed near the snow surface measured in the wind tunnel. A dashed curve is based on original data and a solid straight line is based on corrected original data by d=0.4mm.

transferred to a sintered snow particle and consumed as energy required to break it off from the surface, creating two fresh surfaces at the sintered neck. Since the resulting values ranges from 39 to 55 cm sec^{-1}, he suggested that, if free snow particles exist on the windward surface of snow and acquire a sufficient moving speed to saltate from the wind, they will act as effective triggers to cause the drifting of snow to the leeward. Actually, YAMADA (1974)

Table 2. Summary of the result of wind tunnel experiments

Run	U_0 m/s	wind profile				direct measurement	
		U_* cm/s	$\tau_p=\rho U_*^2$ dyne/cm^2	Z_0 cm	d mm	τ_d dyne/cm^2	$U_*'=\sqrt{\frac{\tau_d}{\rho}}$ cm/s
A	4.7~5.0	36.6	1.88	0.015	0.9	2.8	44.7
B	3.9~4.5	22.6	0.72	0.0022	0	1.8	35.8
C	8.0~8.5	48.7	3.32	0.01	2.0	8.3	77.0
D	11.2~11.3	64.4	5.81	0.006	0.4	15.6	109
E	15.9~16.3	113	17.9	0.017	1.0	30.7	159
F	18.6~19.9	167	39.1	0.047	1.5	43	175

U_0 : wind speed at center of the tunnel, U_* : friction velocity, τ_d : shear stress,
Z_0 : roughness parameter, d : zero-displacement, τ_d : shear stress,
U_*' : friction velocity, ρ : air density

b

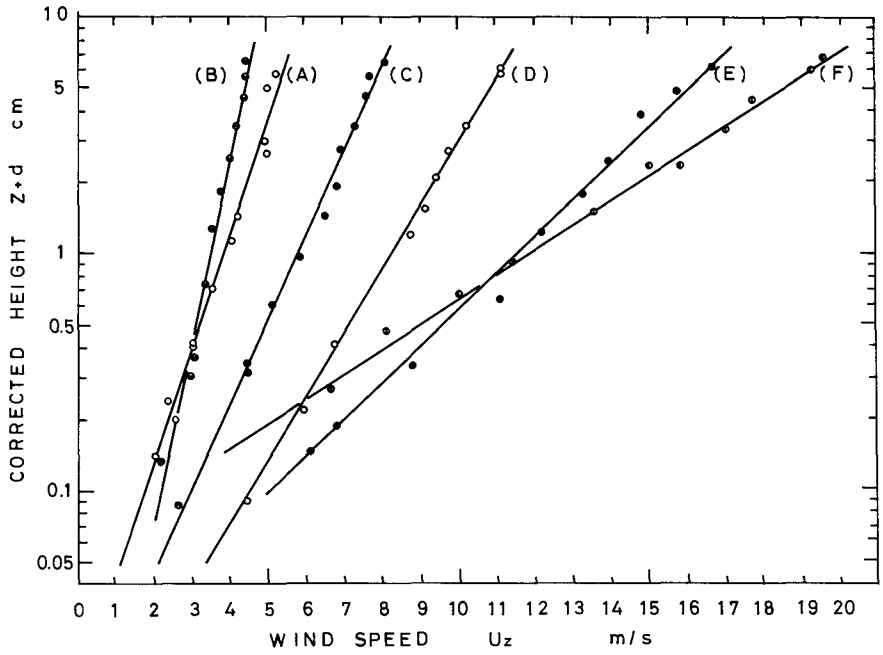

Fig. 35 Wind speed profiles in the wind tunnel corrected by d near the snow surface.

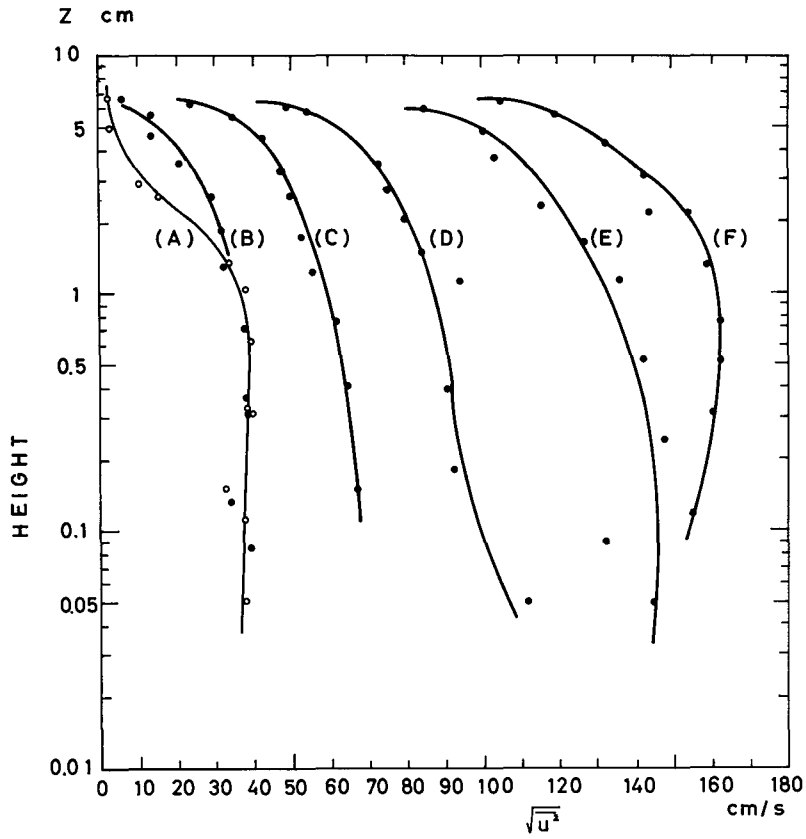

Fig. 36 Profiles of standard deviation of wind speed near the snow surface in the wind tunnel.

reported of a photograph which shows the generation of drifting snow at a site on the windward side of about 20 cm high sastrugi in Antarctica.

V. 3. *Wind structures near the snow surface*

When the surface is made of porous media as in the case of snow, the so-called zero-plane displacement d is introduced into equation (1) as an additional parameter. Equation (1) is then rewritten as

$$U_z=(U_*/K)\ \ln\ (Z+d)/Z_0. \tag{6}$$

The zero-plane displacement is caused by the wind speed below the snow surface, so $U_z=0$ on $Z=Z_0-d$. An example of vertical distribution of wind speed near the snow surface is shown in Figure 34, in which a dashed curve shows that the vertical wind profile is no longer straight.

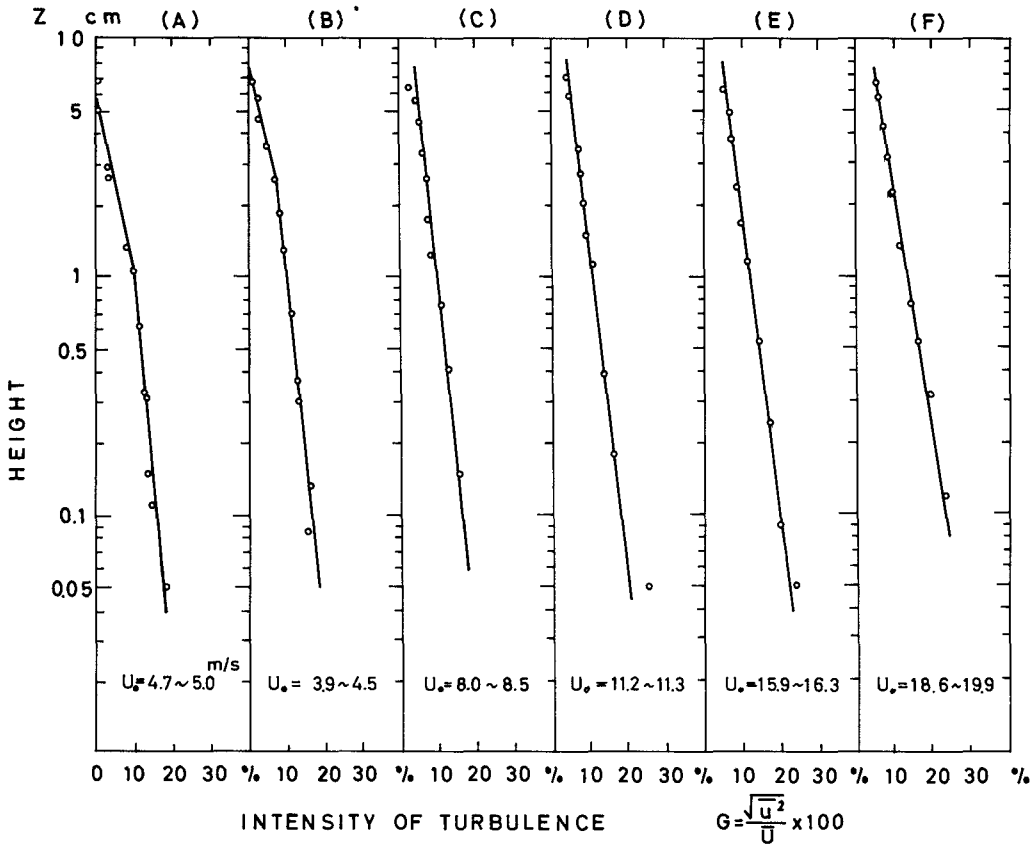

Fig. 37 Profiles of intensity of turbulence near the snow surface in the wind tunnel. U_0: wind speed measured at center of the wind tunnel.

The best value of d was 0.4 mm to have original data corrected and a straight line obtained in this figure. ÔURA et al. (1967), who placed a hot-wire anemometer at the depth of 0.5 cm below the snow surface, found that the wind speed mesured was not zero, but more than 0.3 m sec^{-1}. Making a theoretical study of the air flow induced in a snow cover by the blowing of wind over its surface, YOSHIDA (1977) showed that the air flow can be decomposed into two component flows; i.e., a steady flow which drags the surface of snow with a shear stress and a turbulent flow which pushes the surface with a fluctuating pressure. A series of measurements of a wind profile near the surface disclosed d was in the range between 0 and 2.0 mm, as shown in Table 2. Wind profiles corrected by d are shown in Figure 35. Also, obtained by the measurements using a hot-wire anemometer, were profiles of standard deviation of wind speed fluctuation denoted by σ_u and profiles of intensity of wind turblence on gustiness which is denoted by G, and defined by equation (7), which is written as

$$G=(\sqrt{u'^2}/U)\times 100=\frac{\sigma_u}{U}\times 100(\%), \tag{7}$$

where u' is the fluctuation of wind speed and U the mean wind speed at a measuring point. The results are shown in Figures 36 and 37.

In most cases, σ_u decreases sharply with height near the layer of the surface, and increases with wind speed near the surface. The intensity of turbulence also decreases linearly with height and was almost 20 % near the surface independent on wind speed. These turbulence quantities such as the standard deviation of wind speed fluctuation σ_u and gustiness G near the snow surface relate at least to the generation of drifting snow. From the result in wind-tunnel test, the thershold value of σ_u regarding generation of drifting snow was 0.7 m sec^{-1}.

VI. Structures of wind turbulence during a snowdrift

VI. 1. *Method of data analysis*

Unfortunately, we do not have a fairly precise knowledge of turbulence in drifting snow. Calculations were made in this chapter mainly of standard deviations, correlation coefficients, and power spectral densities and co-spectra of wind speed fluctuation measured by sonic anemometers during the drifting of snow, using the following procedures outlined by BLACKMAN and TUKEY (1958):

(1) A long-period fluctuation in wind speed components is eliminated by a high-pass filter as follows:

$$\begin{aligned} y_i=x_i-\frac{1}{m^2}\ &(x_{i-m+1}+2x_{i-m+2}+\cdots\cdots+(m-1)x_{i-1} \\ &+mx_i+(m-1)x_{i+1}+\cdots+x_{i-m-1}), \end{aligned} \tag{8}$$

where x_i is the value of fluctuation of either the horizontal speed u_i or the vertical speed w_i, at the i-th sampling time, i.e. i times Δt (Δt=0.2 sec), y_i is the out put of the filter, m is the number of lags, and $i=1, 2,\cdots\cdots N$.

In practice the following recurrence formulas are used instead the above equation so that the computing time is reduced:

$$y_{i+1}=y_i+x_{i+1}-x_i+\frac{1}{m^2}V_{i+1} \tag{9}$$

$$V_{i+1}=V_i-X_{i-m}+2X_i-X_{i+m} \tag{10}$$

wher m = 10.

If m=10, the output power falls off the 0.35 times the input power at 0.2 Hz,and 0.036 times at 0.1 Hz, but for the input power at more than 0.4 Hz,there is no change between the output and the input power.

(2) Autocorrelation and cross-correlation coefficients are caluculated for u_i and w_i, each of which stands for the values subtracted by a fluctuation less than 0.2 Hz, using the following equations :

$$R_{uu}(j)=\frac{1}{N-j}\sum_{i=j}^{n-j} u_j \cdot u_{i+j}=<u_i \cdot u_{i+j}>_i, \tag{11}$$

$$R_{ww}(j)=<w_i \cdot w_{i+j}>_i, \tag{12}$$

$$R_{uw}(j)=<u_i \cdot w_{i+j}>_i, \tag{13}$$

$$R_{uw}(-j)=<w_i \cdot u_{i+j}>_i, \tag{14}$$

where i=1. 2,……N; j=0, 1,……, M.

(3) The spectrum function is a cosine transformation of the autocorrelation function, whereas a consine transformation of the cross-correlation function is given by the following equation:

$$F_u(n)=\delta_n <R_{uu}(j)\cdot\cos\frac{n\pi j}{M}>_j, \tag{15}$$

$$F_w(n)=\delta_n < R_{ww}(j)\cdot\cos\frac{n\pi j}{M}>_j, \tag{16}$$

$$CO_{uw}(n)=\delta_n <\frac{R_{uw}(j)+R_{uw}(-j)}{2}\cos\frac{n\pi j}{M}>_j, \tag{17}$$

$$Q_{uw}(n)=\delta_n <\frac{R_{uw}(j)+R_{uw}(-j)}{2}\sin\frac{n\pi j}{M}>_j, \tag{18}$$

where j, n=0, 1,……M;

$\delta_n=\frac{1}{2}$ at n=0, M;

δ_n=1 at n=0.

(4) The given spectra are smoothed out through a "hamming window" in the following equation:

$$\left.\begin{aligned} y_0&=0.46x_0+0.46x_1\\ y_i&=0.23x_{i-1}+0.54x_i+0.23x_{i+1},\ 1\leqq i\leqq M-1,\\ y_m&=0.46x_{m-1}+0.46x_m, \end{aligned}\right\} \tag{19}$$

where x_i and y_i are an input and an output value of a spectrum respectively. When smoothed out, $F_u(n)$, $F_w(n)$, $CO_{uw}(n)$, and $Q_{uw}(n)$ are called respectively power spectrum of u_i, power spectrum of w_i, cospectrum and quadrature spectrum. Using these spectra, the coherence $CH(n)$ and the phase lag $Y(n)$ are defined in the following equations:

$$CH(n)=\frac{CO_{uw}(n)^2+Q_{uw}(n)^2}{F_u(n)\cdot F_w(n)} \tag{20}$$

$$Y(n)=\tan^{-1}\left(\frac{Q_{uw}(n)}{CO_{uw}(n)}\right) \tag{21}$$

The cospectrum $CO_{uw}(n)$ is a display of $CO_{uw}(n)$ versus the frequency n, where $\int_0^\infty c_{uw}(n)\mathrm{d}n=\overline{u_i w_i}$. The coherence, which varies from 0 to 1, is an index of exactness of a relation between the two variables (the horizontal and the vertical variable) of various frequencies.

VI. 2. *Turbulence quantities in drifting snow*

Turbulence quantities such as the standard deviation of longitudinal wind speed σ_u and the intensity of turbulence, i.e., gustiness G, were measured during the drifting of snow by use of sonic anemometer. The standard deviation of wind speed is one of the most important factors which determine the structure of the atmospheric surface layer. In parctical terms, σ_u is a governing parameter which describes the threshold drag force and the behavior of snow particles diffused in the air. A relation between σ_u and wind speed U_1 at the height of 1 m during the drifting of snow are shown in Figure 38. The threshold value of σ_u for generation of drifting of snow was 0.6 m sec^{-1}, which agree with the value of wind-tunnel test. From the figure σ_u is proportinal to U_1^2. Since the standard deviation of vertical wind speed σ_w is linearly proportional to U_* over a wide range of stability conditions (YOKOYAMA et al., 1977), σ_u also may be proportional to U_*. This means that mechanical production of turbulence is more pre-

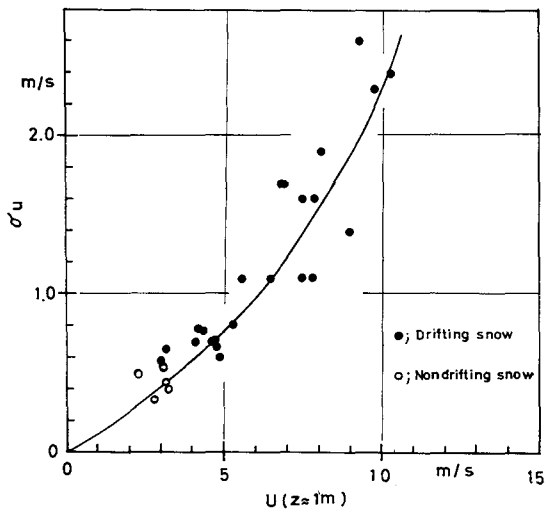

Fig. 38 Standard deviation of longitudinal wind speed during drifting of snow against wind speed at height of 1 m in Sapporo.

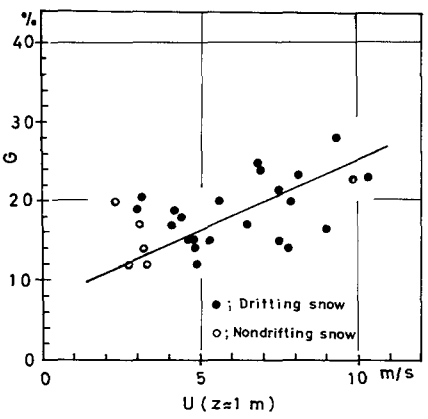

Fig. 39 Intensity of turbulence measured against wind speed at height of 1 m during drifting of snow in Sapporo.

dominant than thermal production of it during the drifting of snow.

GAMO and YOKOYAMA (1975) reviewed the results of other experiments and theories concerning the relation between σ_w and wind speed U above water and flat plains. Using equation (7), if σ_u is prorortional to U_1^2, then the intensity of turbulence G is proportional to U_1. In fact, G tends to be proportional to U_1, as shown in Figure 39.

VI. 3. *Scale of wind turbulence*

According to INOUE (1952), the autocorrelation coefficient $R(t)$ at small time lag t may be approximated by the following equation:

$$R(t)=1-\left(\frac{t}{T_0}\right)^m, \tag{22}$$

where T_0 is the characteristic time taken for the "largest turbulon" to pass through a measuring point and m is the numerical constant. Thus, the scale of the "largest turbulon" L is defined by the following equation:

$$L=T_0 \cdot U, \tag{23}$$

where U is the mean wind speed at a given height. It is noted here that L is always much larger than TAYLOR microscale (e.g., TENNEKES and LUMLEY, 1972) but that it agrees approximately with the integral scale defined by

$$l\equiv\int_0^\infty R_{uu}\, d(t). \tag{24}$$

Examples of autocorrelation coefficients of longitudinal wind speed difting and nondrifting snow, which were obtained in Sapporo, are shown in Figures 40 and 41. They represent a relation between the lag time t and $1-R(t)$. Since t equals T_0 when $1-R(t)$ i unity, each of

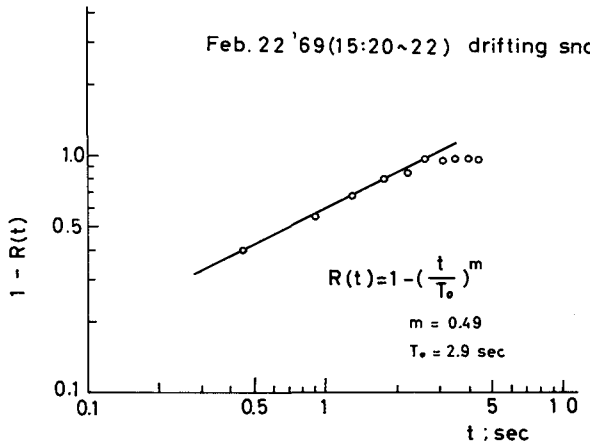

Fig. 40 Autocorrelation coefficients of longitudinal wind speed $1-R(t)$ against time lag t during drifting of snow in Sapporo.

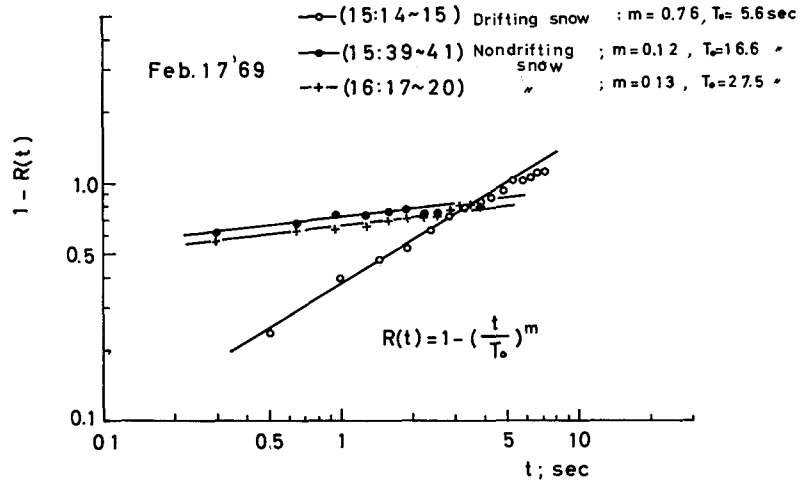

Fig. 41 Autocorrelation coefficients of longitudinal wind speed $1\text{-}R(t)$ against time lag t during drifting of snow (○) and nondrifting of snow (●, +) in Sapporo.

characteristic times is obtained from the point of intersection of a solid line and the line of $1\text{-}R(t)=1$ in the figures. The characteristic times in drifting snow are smaller than those in nondrifting snow. This means that the scales of turbulence in drifting snow are smaller than those in nondrifting snow. On the other hand, the value of m in drifting snow is between $\frac{1}{3}$ and $\frac{2}{3}$ in the prevent paper. According to the theory of a local isotropic turbulence, m is equal to $\frac{2}{3}$ but the value obtained in nondrifting snow was smaller than $\frac{1}{3}$. This means that mechanical production of turbulence tends to weak on because of nondrifting snow. The results from our measurements are summarized in Table 3. The results suggest that the scale

Table 3. Summary of turbulent measurements at Sapporo (1969)

Date	Time	Δt (sec)	Z (cm)	U_z (m/s)	$\sqrt{\overline{u^2}}$ (m/s)	G (%)	T_0 (sec)	$L=U_z\times T_0$ (m)	m	Remarks
Feb. 5	17 : 20~	0.1	85	8.55	1.54	18	1.0	8.6	0.3	blowing snow
Feb.17	15 : 14~15	0.48	73	3.0	0.6	19.8	5.6	17.0	0.76	
	"	0.1	73	3.0	0.59	19.6	5.6	17.0	"	drifting snow
Feb.17	15 : 39~41	0.32	73	2.75	0.37	13.5	16.6	45.6	0.12	
	16 : 17~20	0.32	73	3.2	0.52	16.3	27.5	88.0	0.13	nondrifting snow
Feb.20	14 : 48~50	0.33	68	3.1	0.57	18.1	7.2	22.4	0.43	
	15 : 03~05	0.33	68	4.9	0.59	12.2	2.9	14.2	0.48	drifting snow
	16 : 33~35	0.33	68	4.6	0.67	14.7	3.6	16.2	0.33	
Feb.22	15 : 20~22	0.44	68	4.1	0.72	17.7	2.9	12.0	0.49	drifting snow
Feb.25	14 : 41~43	0.45	69	4.7	0.71	15.2	3.2	15.2	0.37	drifting snow

ΔT : sampling time, Z : height of snoic anemometer, U_z : mean wind speed at Z,
$\sqrt{\overline{u^2}}$: turbulent velocity, G : intensity of turbulence, T_0 : characteristic time,
L : scale of turbulence, m : value of exponent in eq. (22).

of the turbulence L during the drifting of snow was small in comparison with that which was measured during the nondrifting of snow. For example, when the mean wind speed was about 3 m sec^{-1} both in drifting snow and nondrifting snow, the scale of turbulence was about 17 m in the former and approximately 44.6 to 88 m in the latter, on therefore the latter was about 2~5 times that of the former. For the measurement of the scale of turbulence space correlation coefficients have a direct physical meaning. It is difficult however, to obtain space correlation coefficients, because many sonic anemometers are required.

In an effort possible to study the space correlation seven cup-anemometers were placed along the wind direction one each at distances of 0, 2, 5, 10, 20 and 115 m. The sampling time interval of wind fluctuation was 5 sec and the recording time for each run was 5 min. The space correlation coefficient $R(x)$ between any two points with a distance of x, is defined by the following equation:

$$R(x)=\frac{<u(0)\cdot u(x)>_t}{<u^2(0)>_t^{\frac{1}{2}}<u^2(x)>_t^{\frac{1}{2}}}, \tag{25}$$

where the notation $<\quad>_t$ means time average.

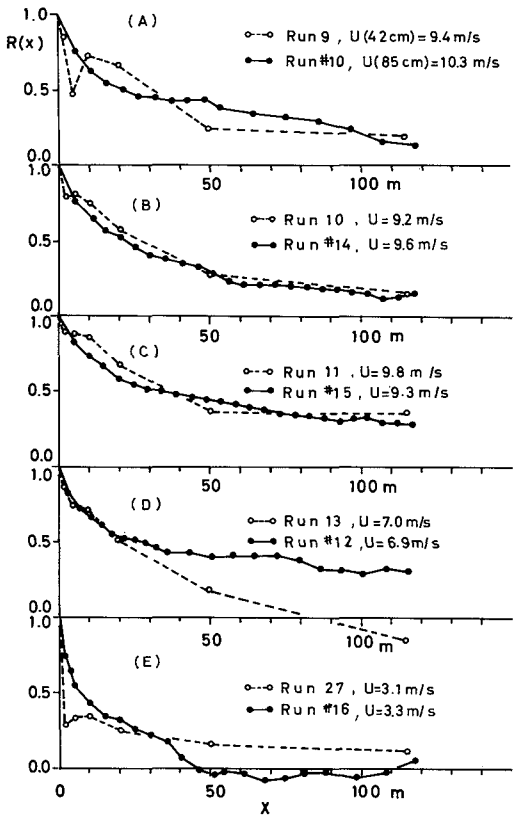

Fig. 42 Space-correlation coefficients $R(x)$ against distance x along the wind direction. A solid line shows $R(x)$ which was derived by use of $X=Ut$ from the auto-correlation coefficient $R(t)$ obtained by a sonic anemometer. A dashed line shows $R(x)$ directly measured by use of seven cup-anemometers.

For comparison between $R(x)$ and the autocorrelation coefficient $R(t)$ obtained by sonic anemometers the latter was converted to $R(x)$ by use of the relation:

$$x=U\cdot t, \tag{26}$$

where U is the mean wind speed and t the time lag.

Figure 42 illustrates a comparison between space-correlation coefficients and those converted from autocorrelation coefficients, showing an approximate agreement between them.

VI. 4. *Relation between snow-wave spacing and wind turbulence scale*

As described in III. 6., snow-waves have wavelengths from 3 to 15 m and eroded patterns like sastrugi and formed in wave troughs. Accordingly, after a snowdrift has been formed, observations can be made of areal variations. We can see partly flatter snow-waves as shown in Figure 43 than those shown in Figure 8 (see III. 6.). Then, snow-waves are seen on the snowfield not only during the drifting of snow but also after drifting ceased, as shown in Figure 44. In addition to these snow-waves, eroded regions (groups of sastrugi) formed on the snowfield were sketched, as shown in Figure 45; i.e., a traverse observation of the snowfield disclosed both eroded and noneroded regions on the snow surface, whereupon measurements were made of the mean distance between two adjacent eroded areas. Each eroded region consisted of groups of small sastrugi. Thus, the wavelegths of snow-wave and the spacings of adjacent eroded regions were nearly of the same order of magnitude as the scale of turbulence calcu-

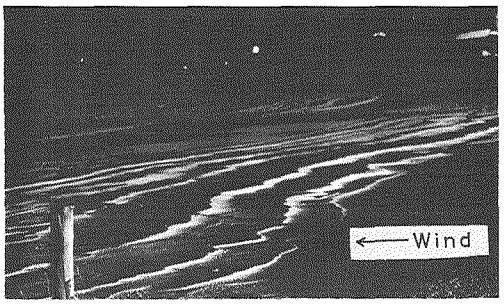

Fig. 43 Photograph of flatter snow-waves taken at night in the illuminated artificial light in Sapporo.

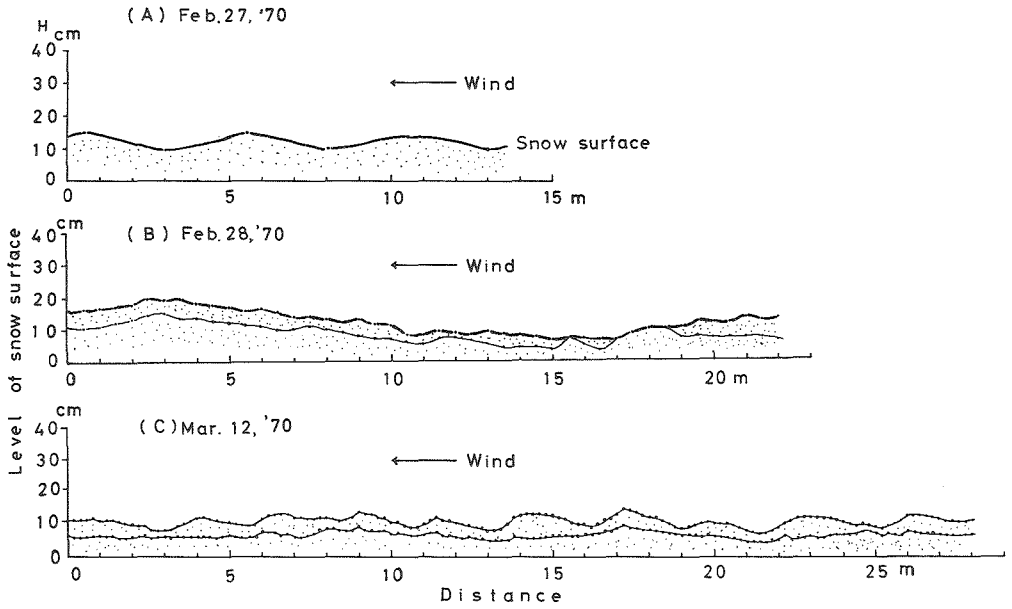

Fig. 44 Examples of sections of snow-waves sketched after drifting snow ceased.

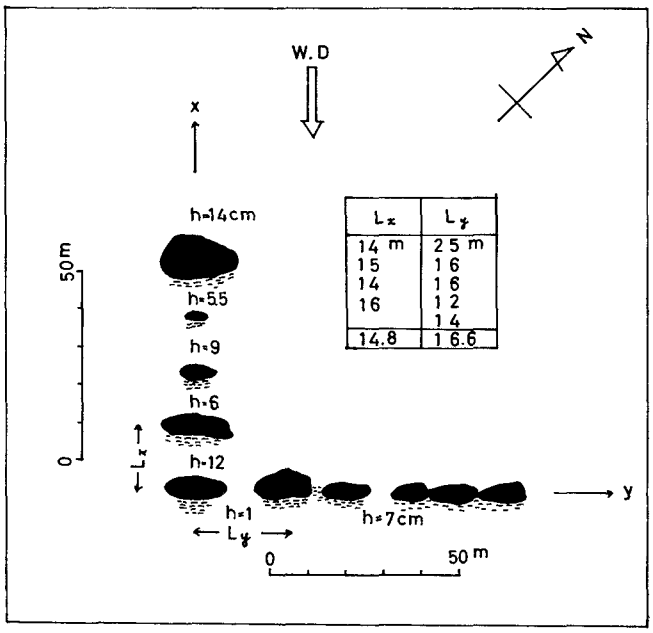

Fig. 45 Sketch of spacings of adjacent eroded regions in the directions longitudinal and transverse to the wind direction. Values of h: depths of a snow cover affected by drifting snow. Tinted portions: small sastrugi.

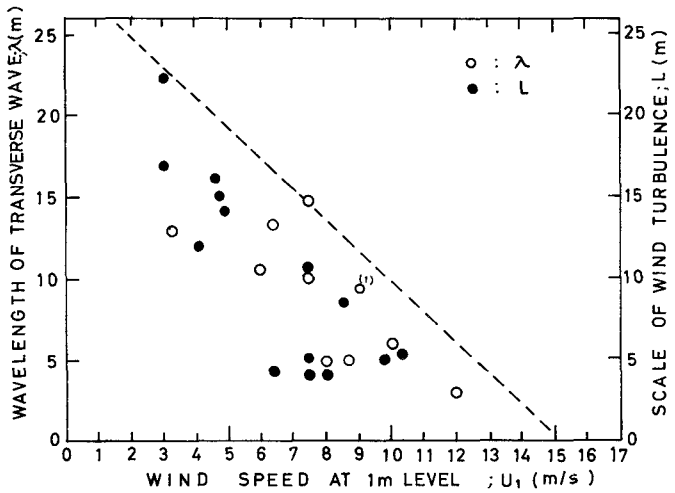

Fig. 46 Relation of wind speed at height of 1 m (U_1) with wavelegth of a transverse snow-wave (●) and scale of wind turbulence (○). (1); A datum obtained by R. NARUSE.

lated by equation (23) described in VI. 3. The results from measurements are shown in Figure 46. The scale of turbulence is clearly in agreement with such scales of patterns marked by erosion on the snow surface as wavelengths of snow-waves or distances between groups of sastrugi. In addition, the scale of turbulence and the spacings of snow-waves vary inversely with the mean wind speed. In particular, the spacings of snow-waves approach zero when the mean wind speed at the height of 1 m above the snow surface rises above 15 m sec^{-1}. This means that a transverse feature will disappear in a strong wind because of the predominance of longitudinal characteristics of the wind. Thus, transverse features (ripples, waves, barchans) occur with winds of under 15 m sec^{-1} whereas longitudinal features (dune, sastrugi) result when winds rise above 15 m sec^{-1}. Observations of drifting snow by DALRMPLE (1966) and YAMADA (1974) in Antarctica support this; according to their observations, the threshold wind speed differentiating between drifting snow (with snow particles moving at low levels) and blowing snow (with snow particles moving at high levels) was 13 to 14 m sec^{-1}. Similar features have been reported in relation to clouds; i.e., clouds, which are aligned perpendicular to the flow in the presence of a weak shear oriented along the direction of the flow, as the shear (MAL , 1930).

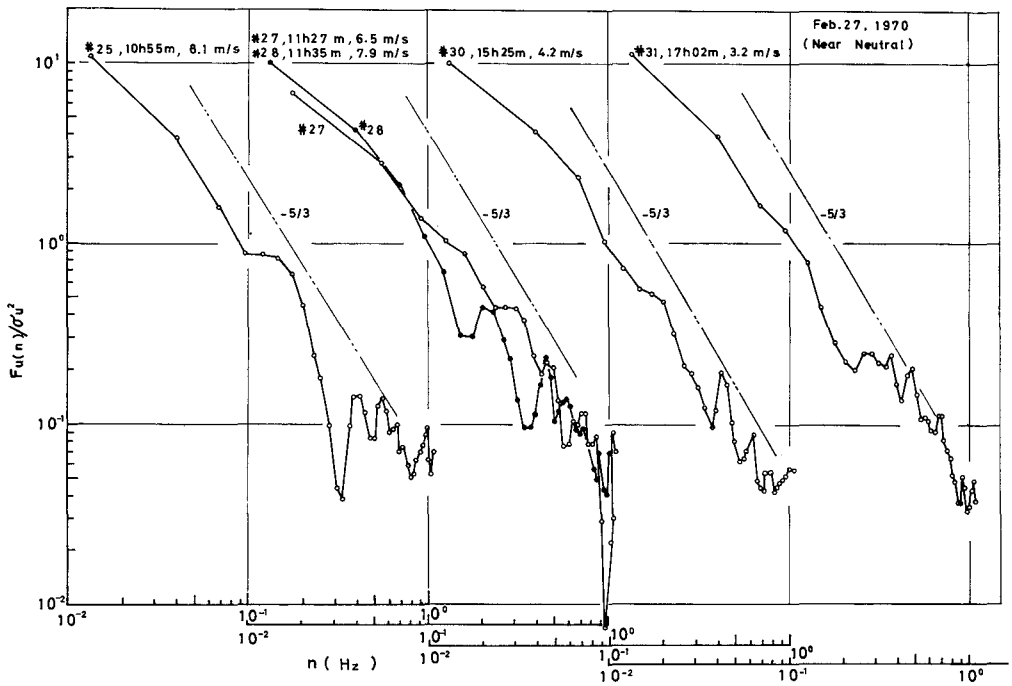

Fig. 47 Normalized power spectral densities of longitudinal component of wind fluctuations during formation of snow-waves.

VI. 5. *Power spectral densities under various snow surface conditions*

Generally speaking, dimensional considerations provide an effective tool for deriving spectral characteristics. One of the most known is KOLMOGOROFF's "$-\frac{5}{3}$" law (BATCHELOR, 1953) for the inertial subrange of turbulent velocity fluctuations. In this subrange where energy transfer is predominantly governed by the rate of energy dissipation ε as well as by the wave-number k, the molecular viscosity ν contributing nothing to it, the spectrum of velocity fluctuations is expressed by

$$F(K)=\alpha\varepsilon^{\frac{2}{3}}K^{-\frac{5}{3}} \tag{27}$$

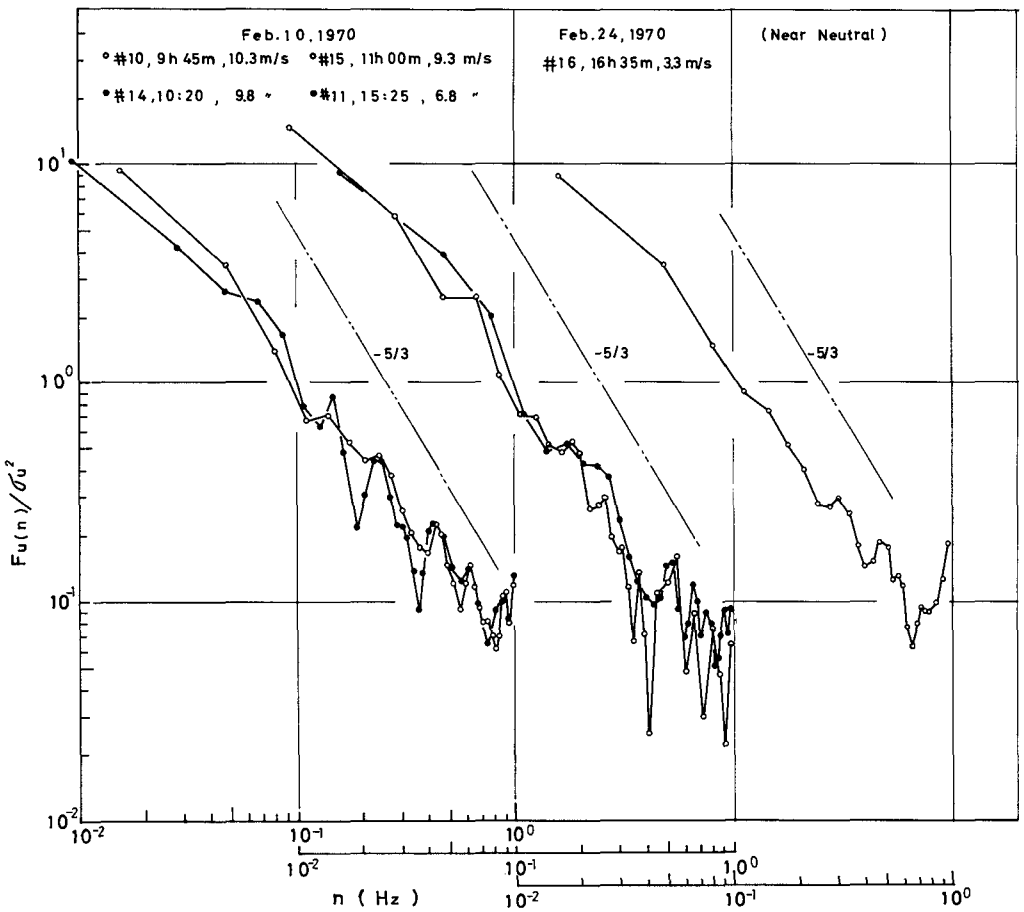

Fig. 48 Normalized power spectral densities of longitudinal component of wind fluctuations during formation of sastrugi.

where α is the universal constant named Kolomogoroff constant.

Normalized power spectral densities of u-component of wind fluctuations during the formation of snow-waves and sastrugi are shown in Figures 47 and 48 respectively. All of these spectrum a nearly follow the so-called "$-\frac{5}{3}$" law in a higher frequency side. Shown in Figure 47 is a change in spectrum with progress of time over snow-waves. It appears that the spectral characteristics of turbulence over the snow-wave have a sharp dip in a higher frequency region, whereas the shape of a spectrum obtained in the absence of drifting snow is comparatively smooth, as shown by Run #16 in Figure 48. However, HIRO (1968) dervided the "-3 power law" and "-2 power law" on the spatial spectrum of sand-waves formed by flowing water for a large wave-number equilibrium subrange, based on a dimesional consideration. He showed also that the spectra agreed with experimental data from various sources (NORDIN and ALGERT, 1966; ASHIDA and TANAKA, 1967; FUKUOKA, 1968).

VI. 6. *Change in coherence and cospectrum during snow-wave formation*

Momentum transfer from air to the snow surface was studied by measuring fluctuations in the horizontal and the vertical wind speed component, using two sonic anemometers at the same height of 135 cm for each component under a condition in which a snow-wave was formed. It was formed when the wind speed at the height of 1 m was more than 7 m sec^{-1} after an accumulation of 20 cm of new snow on a snowfield. Then, the snow-wave had the wavelenght of 10 m and a wave height of 15 to 20 cm. Profiles of temperature and wind speed at time of formation of a snow-wave are shown in Figure 49 (a) and (b), respectively. The former was obtained under a neutral condition. As for the latter plotted on a semilog scale, a dashed and a solid line represent noncorrected and corrected plots of wind speed by the zero-plane displacement assumed to be 20 cm. Figure 49 (b) shows also that, when a transverse snow-wave is being formed, the wind shear near the snow surface is weakened.

Fluctuations in wind speed were recorded on a chart running at the speed of 1 cm sec^{-1}. Values of wind speed were read at the interval of 0.25 sec, each run having the duration of 2 min, because the phnomenon of drifting snow occur very quickly. An example of coherence during a snow-drifting period, the case of period (1) in Figure 14, is shown in the middle section of Figure 50. A remarkable peak is seen at the frequency of 0.7 Hz marked with an asterisk in it. The snow-wave had the computed length of 10 m, which agreed with the observed wavelength of the snow-wave. On the other hand, when the process of snow-wave formation was weakened in the case of period (2), as shown in Figure 14, a frequency peak is not seen though snow was drifting (see Figure 51).

The co-spectrum, which is related to momentum transfer, also had a peak at the frequency of 0.7 Hz (marked with an asterisk in the upper section of Figure 50), corresponding to the wavelength of the snow-wave. Dominance of upward transfer of momentum seen in it suggests that wind turbulence and snow-wave formation interact with each other. Here it should be noted that there is poor statistical reliability of spectra from a data obtained only for a

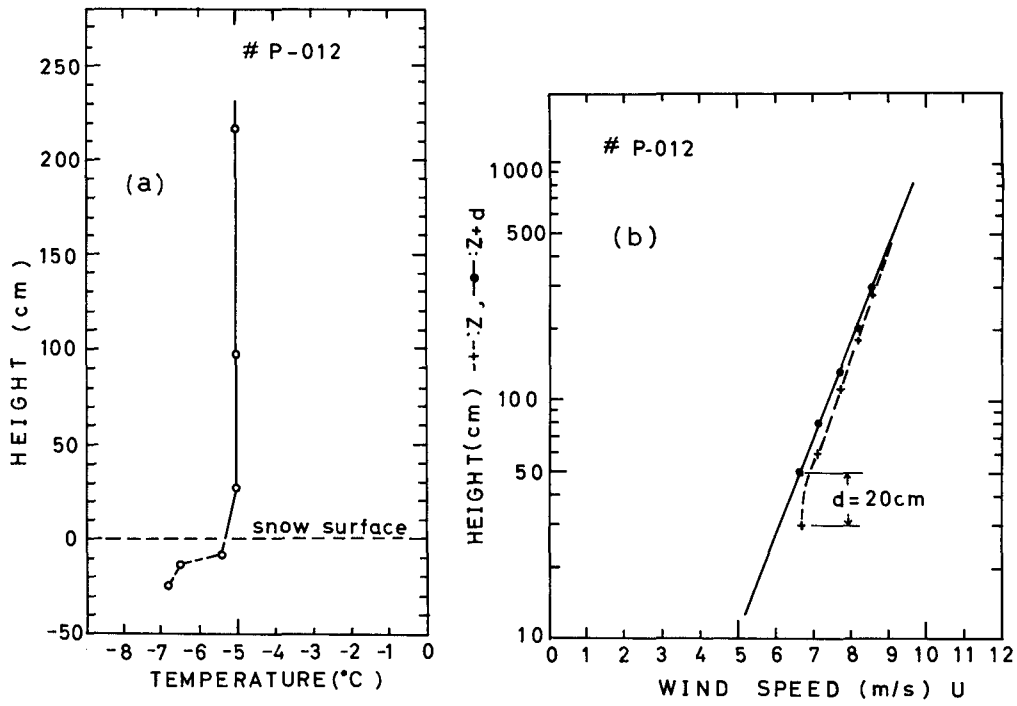

Fig. 49(a), (b) Profiles of temperature (a) and wind speed (b) under a snow-wave forming condition.

duration of two minutes, because of a slow movement of the wave. If a single peak, with the freedom of 10 deg, is observed to be 9 cm^2 sec^{-2} Hz^{-1} as shown in Figure 50, then it is supported a level of cnfidence that the true long-run value lies between 5.0 and 16.3 cm^2 sec^{-2} Hz^{-1}. Apart from it, there is a physical explanation of the peak frequency which corresponded to the wavelength of the snow-wave observed.

ASAI (1970) made an investigation of three-dimesional features of perturbation by superimposing a plane Couette flow with a flow of unstable stratification. He showed that the transfer a vertical momentum tends to be made upward against a shear for a transverse perturbation, while it tends to be made downward for a longitudinal perturbation. This indicates that a transerse perturbation transforms the kinetic energy of perturbation to that of the mean flow through an upward transfer of a horizontal momentum against a shear. However, Asai's work would be looked on as irrelevant to the present study because it pertains to unstable conditions, whereas the data over the snow dealt with neutral conditions. Another possibility may be the "fluidization of snow" caused by wind action (KUROIWA, 1975). A snow cloud associated with an avalanche or heavy blowing presents an example of fluidized snow, whose dynamic behavior has been investigated very actively (MAENO and NISHIMURA, 1978,1979). The result described above, however, agrees with the result described in Ⅵ. 4.

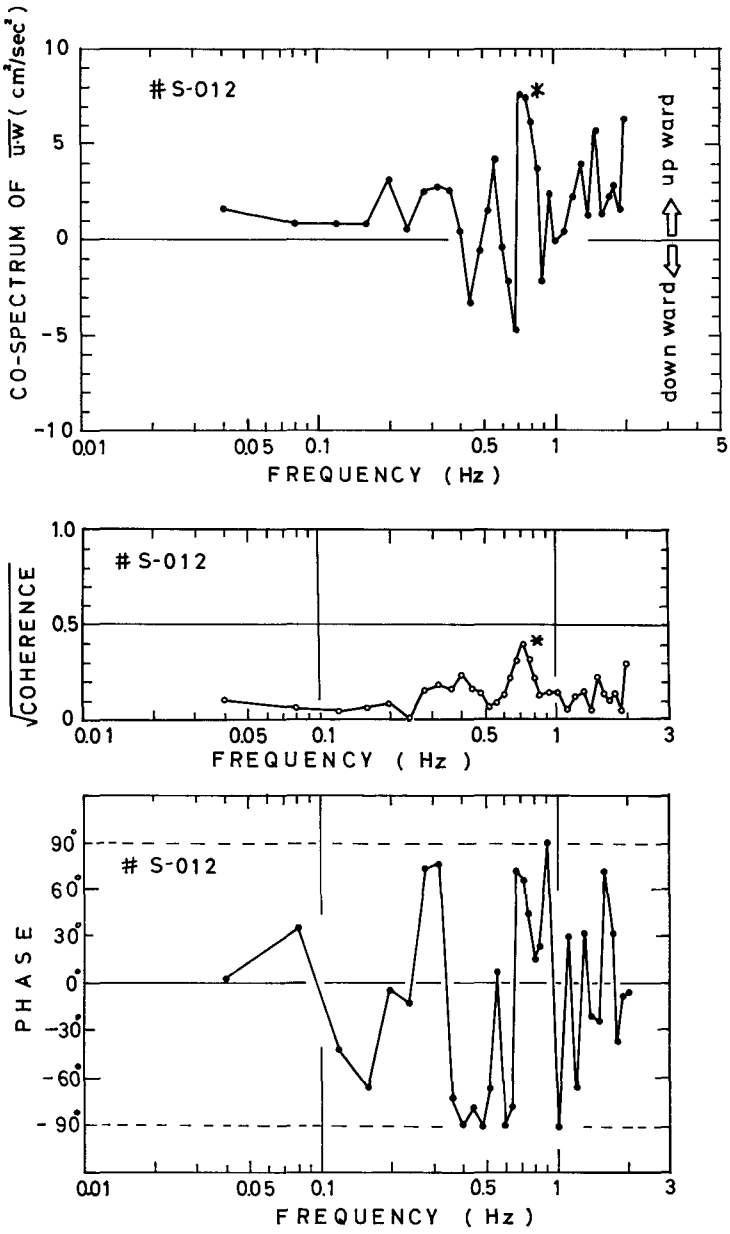

Fig. 50 Cospectrum, coherence and phase angle of covariances *uw* under an active snow-wave forming condition.

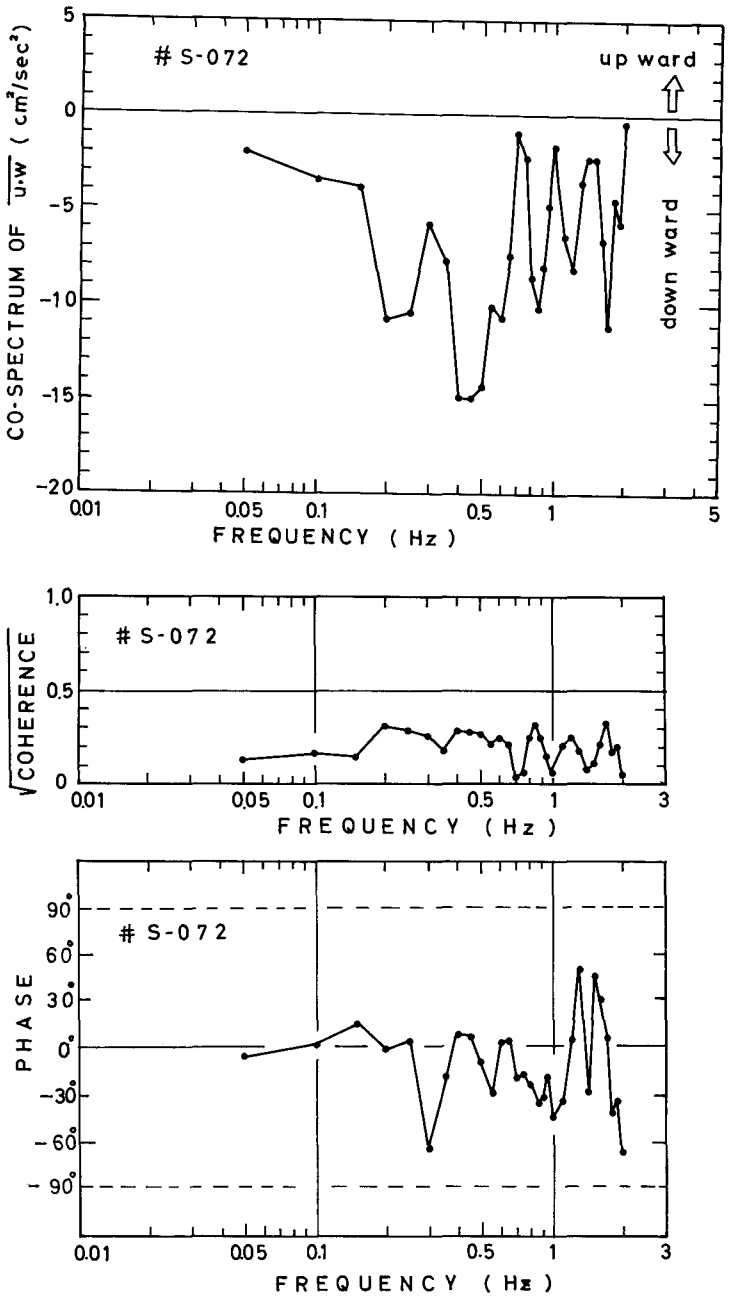

Fig. 51 Cospectrum, coherence and phase angle of covariances uw under a stable surface condition 40 min after ending of active wave formation in Fig. 50.

VI. 7. *Some characteristics of turbulence on a hard snow surface at Mizuho Station*

As examples of autocorrelation coefficients, those obtained at Mizuho Station are shown in Figure 52, which shows a relation between the lag time t *and* $1-R_j(t)$ $(j=u,v,w)$. The characteristics times, which are obtained from the figure and shown in Table 4, are of the same order of value as those obtained in drifting snow in Sapporo. According to these charactristics times, the mean scale of the "largest turbulon" (INOUE, 1952) represents a long and narrow visionary vortex like an ellipsoid having the dimensions of length, breadth, and height in 3.7 : 2.3 : 1.

Meanwhile, four examples given in Figures 53 (a)~(d) show normalized power spectral densities of vertical wind speed fluctuation and air temperature fluctuation obtained in a period of drifting snow at Mizuho Station. One of the discrepancies in spectrum in the high frequency side; i.e., the former nearly follows the so-called "$-\frac{5}{3}$" law in the high frequency region, whereas the latter approximates to $n^{-\frac{1}{2}}$ on the high frequency side. There is another discrepancy in spectrum, i.e. the depression of a peak at the low frequency side in the vertical wind component (see Run M2 and Run M4) present in the neighbourhood of the BRUNT-VÄISÄLÄ frequency denoted by N which is given by

$$N=\left(\frac{g}{\theta}\frac{\Delta\theta}{\Delta Z}\right)^{\frac{1}{2}}, \tag{28}$$

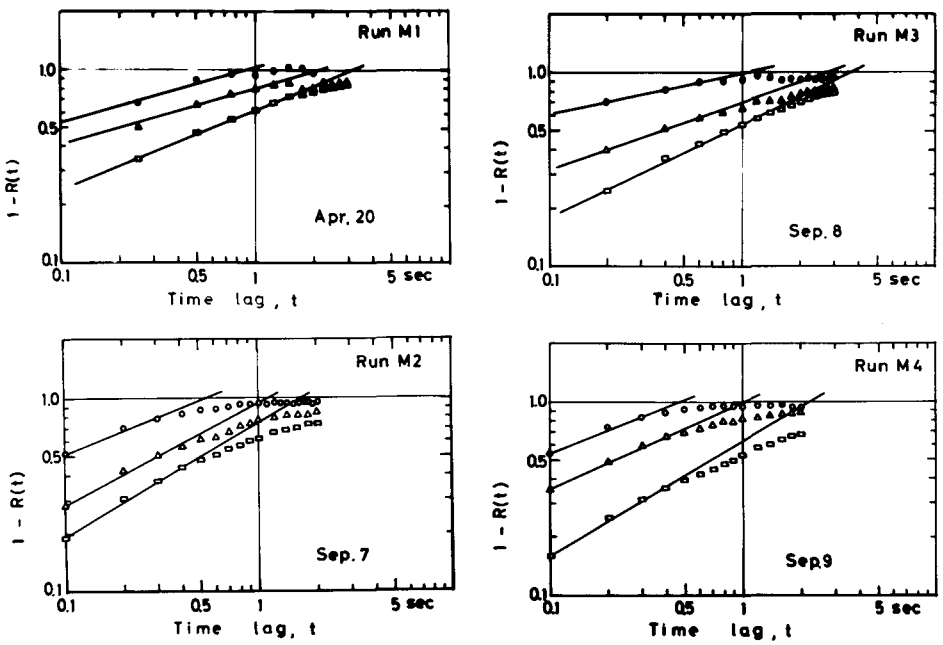

Fig. 52 Autocorrelation coefficients of longitudinal (□), lateral (△) and vertical (○) wind speed 1-R(t) against time lag t in a stationary katabatic wind obtained at Mizuho Station.

Table 4. Mean and turbulent paramenters obtained at Mizuho Station

Run	Date 1973	Time (L.T.)	U(4.5m) m/s	U_* m/s	R_i(3 m)	σ_u σ_w σ_v m/s	σ_w/U_*	T_u T_v T_w sec	m_u m_v m_w
M 1	Apr.20	1810−1815	13.2	0.58	0.003	1.18, 0.93, 0.72	1.24	3.0, 2.1, 0.9	0.42, 0.30, 0.28
M 2	Sep. 7	1409−1514	15.5	0.61	0.004	1.29, 0.94, 0.78	1.28	1.6, 1.1, 0.5	0.60, 0.53, 0.40
M 3	Sep. 8	0970−0915	10.2	0.38	0.024	0.66, 0.53, 0.45	1.18	3.7, 2.7, 1.1	0.48, 0.36, 0.21
M 4	Sep. 9	1458−1505	15.2	0.56	0.004	1.32, 1.03, 0.75	1.34	2.2, 1.0, 0.5	0.59, 0.46, 0.41

U_* : Friction velocity, R_i : Gradient Richardson number, $\sigma_u, \sigma_v, \sigma_w$: Standard deviations of wind velocity (u, v, w : representing respectively longitudinal, lateral and vertical components), T_u, T_v, T_w : Characteristic times (u, v, w : same as above), m_u, m_v, m_w : Values of exponent in eq. (22) (u, v, w : same as above).

where g is the acceleration of gravity, θ is the mean absolute potential temperature of a layer and $\Delta\theta/\Delta Z$ is the vertical air temperature. The so-called "BRUNT-VÄISÄLÄ" frequency is indispensable in all studies of stably stratifield media.

In recent years, wavelike motions have been frequently observed in stably stratified atmospheric conditions; the interpretation of atmospheric data obtained in such conditions may well be complicated by the coexistence of two types of motions, i. e. turbulence and internal gravity waves. One way of distinguishing between the two was proposed by AXFORD (1971) who drew on spectral characteristics of temperature and velocity fields. Meantime, CAUGHEY and REACINGS (1975) described a wavelike phenomenon within 183 m above the earth's surface during nocturnal inversions over land; according to their results, all the spectra have pronounced peaks in the frequency range of $0.002 < n < 0.003$ Hz corresponding to a period lying between 5 and 8 min. The value of 0.002 Hz given by SETHURAMAN (1977) for internal gravity waves at the height of 23.5 m over the ocean in surface-based inversions is in agreement with the above results. The values obtained by the author are, however, larger than those of the above results. The peaks may be shifted to the high frequency side when strong shears are present. Using instrumented aircraft, MASCART et al. (1978) reported that the frequency of a peak is close to 0.03 Hz, within a low-level inversion where the gradient Richardson number is small, i.e., shear production is present.

The "$-\frac{5}{3}$" law is rarely seen applicable to temperature spectra, the exception being shown in Figure 53(a). In general, the slope of a spectrum in a stable surface layer began to approximate to $n^{-\frac{3}{2}}$ (KAIMAL, 1973; RAYMENT and CAUGHEY, 1977). In Figure 61 arrow denote the positions of BRUNT-VÄISÄLÄ frequencies. The peak in the neighbourhood of frequency is not remarkable in Runs M1 and M3. Since the observed frequencies of any wave will have been Doppler-shifted by the mean flow (CAUGHEY, 1977), it cannot be expected that this frequency will correspond to the position of an internal gavity wave a strong shear is present in a flow.

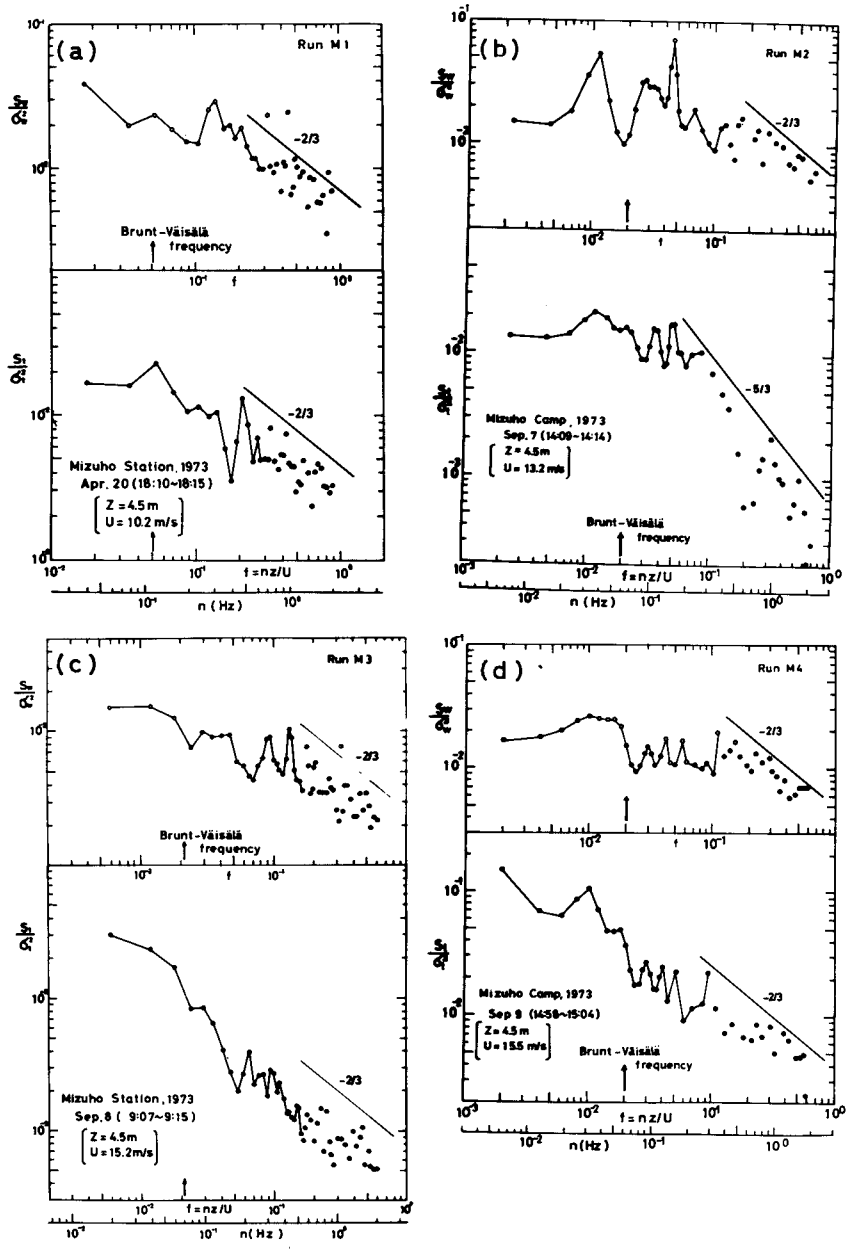

Fig. 53(a)~(d) Normalized power spectral densities of vertical wind speed fluctuation and temperatures fluctuation against nondimensional frequency $f = nz/U$ and frequency n in a stationary katabatic wind obtained at Mizuho Station. Arrows denote positions of BRUNT-VÄISÄLÄ frequency.

Ⅶ. Wind turbulence and a snowdrift around an obstruction

Ⅶ. 1. *Instruments and methods*

A study of wind-snow interaction in connection with snow-drift formation is of great pratical importance to the settling of problems caused by neary snow presipitations and frequent occurrence of strong wind and blowing snow in snowy regions. For this reason the interaction was looked into by observing turbulent fluctuations in horizontal velocity component and vertical distributions of horizontal snow fluxes around obstacles, using two sonic anemometers and three drift collectors in Sapporo. In addition, as an example of large-scale phenomena wind turbulence measurements were conducted at the bare ice field near the Yamato Mountains from December 1 to 7, 1973, using a sonic anemometer as already described in Chapter Ⅱ.

A drawer-type collector consisting of a chest with ten drawers was devised so that it was placed in drifting snow to be withdrawn in such a short time as about 2 minutes, whereby measurements were made of the mass flux of drifting snow. The ten drawers are arranged in a column, one on top of another, between the bottom of the chest and the top of it 1 m in height, as illustrated in detail in Figure 54. The collection efficiency can be assumed to be given by the following equation:

$$\eta = \eta_1 \cdot \eta_2 \tag{29}$$

when η_1 is the aerodynamic efficiency, which shows the efficiency of collection of snow particles at the inlet of the collector and is estimated from a wind-tunnel calibration, while η_2 is the separation efficiency in this collector, which is expressed by the ratio of the total mass of snow particles remaining in the collector (not escaping therefrom) to the total mass of snow particles that have entered the collector. The aerodynamic efficiency is approximated by the following equation:

$$\eta_1 = U_i / U_0, \tag{30}$$

where U_i is the wind speed in the inlet tube of the collector and U_0 is the wind speed at the center of the wind-tunnel. The aero-

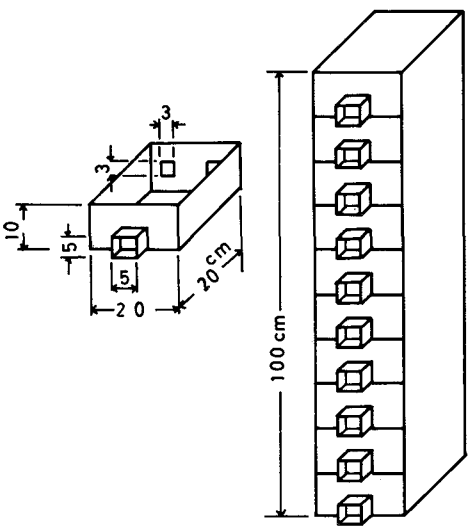

Fig. 54 Drawer-type collector measuring horizontal flux of drifting snow.

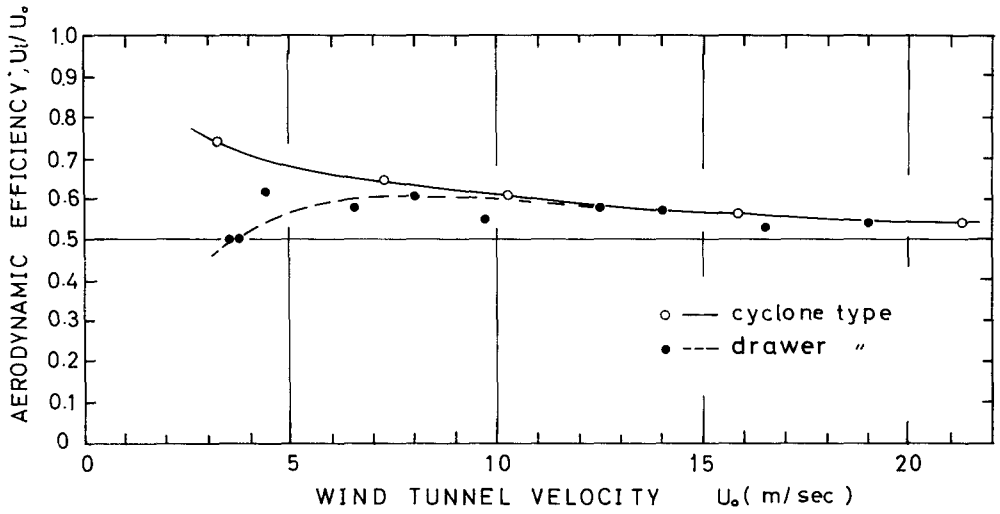

Fig. 55 Aerodynamic efficienty of drift collectors calibrated in a wind tunnel.

dynamic efficiency U_i/U_0 is plotted against U_0, as shown in Figure 55. The aerodynamic efficiency corresponding to the wind speed of 10 m sec^{-1} or thereabout was determined to be 0.6 from the wind-tunnel calibration.

For the determination of the separation efficiency η_2 for the drawer-type collector, a cyclone-type collector (Figure 56) with known separation efficiency ($\eta_2=1$) was used for a comparison between it and the drawer-type collector. As for the aeradynamic efficiency of the cyclone-type collector it was also 0.6 for the wind speed of 10 m sec^{-1} according to the wind-tunnel calibration as shown in Figure 55.

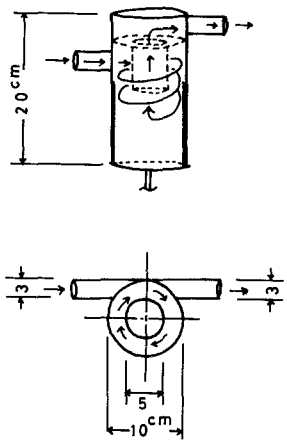

Fig. 56 A cyclone-type collector.

A comparison of collection efficiency between the cyclone-type and the drawer-type collector was tried on a snowfield in Sapporo when snow was drifting. The results are shown in Table 5. The actual mass fluxes collected by both the collectors are given as follows:

$$Q_F=0.6 \cdot \eta_2 \cdot Q, \tag{31}$$

$$Q_W=0.6Q, \tag{32}$$

Table 5. Comparison of collection efficiency between cyclone type and drawer type drift collections

Q_W g cm^{-2} s^{-1}	Q_F g cm^{-2} s^{-1}	Q_W/Q_F obs.	$1+v^2/rg$ cal.	η_2 obs.	η_2 cal.	Wind speed m/s	Height cm
2.3 × 10	0.73 × 10	3.2	2.9	0.31	0.34	8.0	12
0.55 × 10	0.25 × 10	2.2	2.1	0.45	0.48	6.0	10
0.88 × 10	0.33 × 10	2.7	2.4	0.37	0.42	7.0	9
0.52 × 10	0.20 × 10	2.7	2.1	0.37	0.48	6.0	9

where Q_F and Q_W are the values measured of the actual mass flux of the drawer and the cyclon-type collector respectively, and Q is the mass flux in the air. The ratio of Q_F to Q_W is equal to η_2 for the drawer type; namely,

$$\eta_2 = Q_F/Q_W \tag{33}$$

On the other hand, the effective gravitational force F for separation in the case of the drawer type collector is expressed by the following equation:

$$F=(\frac{\pi}{6})d^3(\rho_s-\rho)g, \tag{34}$$

where d is the diameter of a snow particle wich is assumed to be spherical, ρ_s is the density of the particle, ρ is the air density and g is the gravitational acceleration. In the cyclone-type collector, the effective separation force is a centrifugal force because snow particles rotate in the chamber of the cyclon. Therefore, the centrifugal force W is expresed as follows:

$$W=(\frac{\pi}{6})d^3(\rho_s-\rho)\frac{V^2}{r}, \tag{35}$$

where r is the radius of movement in which the particles have the tangential velocity V. Practically, the value of r used the radius of center in the chamber of the cyclone (r=3.75 cm) and V is the value of wind speed at the inlet of the cyclone. The ratio of W to F shows that the centrifugal force is V^2/rg times the gravitational force as in equation (36):

$$W/F = V^2/rg. \tag{36}$$

In the cyclone-type collector, an effective separation force is composed of both the centrifugal and the gravitational force. The ratio of Q_W to Q_F, therefore, will be assumed to be as follows:

$$Q_W/Q_F \sim \frac{F+W}{F} = 1+\frac{V^2}{rg}. \tag{37}$$

Accordingly, from equations (33) and (37), the separation efficiency of the drawer-type collector is expressed theoretically by:

$$\eta_2 = \frac{Q_F}{Q_W} \sim (1+\frac{V^2}{rg})^{-1}. \tag{38}$$

It is decided from Table 5 that the observed mean separation efficiency derived using equation (33) for the drawer-type collector was 0.38, whereupon its value agreed with the calculated mean value drawer-type collector was 0.23 (=0.6x0.38).

The total drift transport in a unit time through the vertical surface of a unit width perpendicular to the wind direction is obtained by integrating mass fluxes $q(z)$ along the height. Then, the rate of snow transport per unit width of the flow Q between two given heights Z_1 and Z_2 is

$$[Q]_{z_1}^{z_2}=\int_{z_1}^{z_2} q(z)dz. \tag{39}$$

Using the drawer-type collector, KOBAYASHI and YOKOYAMA (1977) measured the total drift transport obtained by extrapolating mass fluxes up to the height of 10 m in Antarctica. NARUSE (1970) obtained the drift transport using cyclone-type collectors in August, 1969, on the coastal region of the Antarctic continent near Syowa Station. Again, INOUE and FUJINO (1977) measured the drift transport, whereby the collection efficiency was raised to the value of 0.6.

Ⅶ. 2. *A snowdrift and drift density around an obstruction*

Vertical distributions of horizontal snow mass flux up to the height of 1 m were measured using three drawer-type collectors around a snowdrift, the so-called "wind scoop" (SELIGMAN, 1962) caused by obstruction. A plan of a wind scoop around two small huts and the locations of the collectors are shown in Figure 57. A helicoidal stream around the huts shown in the plan was observed by the trajectories of smoke and drifting snow particles. Collectors are located at places marked by +, ● and ○, showing features of the places, i.e., a flat place windward, a depositional place and an eroded place respectively, corresponding to n_{rf}, n_d and n_e, which represent the snow drift density at each place. Figure 58 shows variations in depth of a snowdrift measured along leeward against the huts corresponding to the direction X in Figure 57.

The data of mass flux $q(z)$ corrected by the value of collection efficiency 0.23 at various heights were obtained simultaneously at three sites shown in Figure 57.

As known well, SHIOTAI and ARAI (1953) and LOEWE (1956) considered stationary conditions in which turbulence transports upwards as much snow particles as settle down under the influence of gravity. The turbulent diffusion equation reduces to the following:

$$w\cdot n+K(\partial n/\partial z)=0, \tag{40}$$

where w is the fall velocity of snow particles, n is the particle concentration or drift snow density (mass of snow per unit volume of air) at the height z, and K is the eddy viscosity (eddy diffusivity), for turbulent winds, which can be expressed by:

$$K=k\cdot U_*\cdot z, \tag{41}$$

where U_* is the friction velocity velocity and k is the von Karman's constant (=0.4). Then the

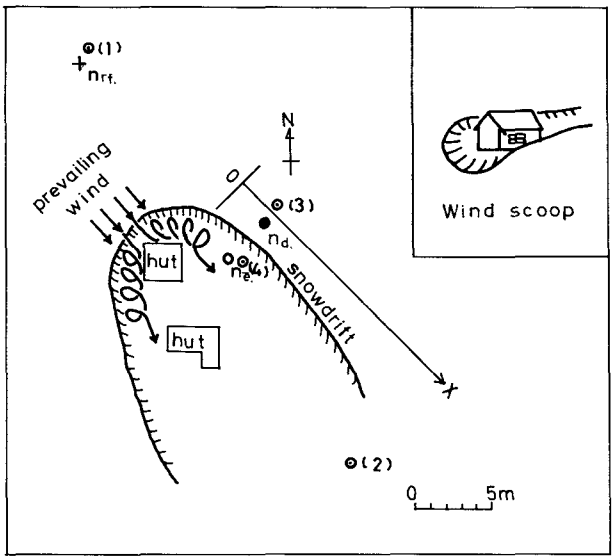

Fig. 57 A plan of wind scoop around two small huts, with locations of collectors n_{rf} (+), n_d (●), n_e (○) and of sonic anemometers (1)-(4).

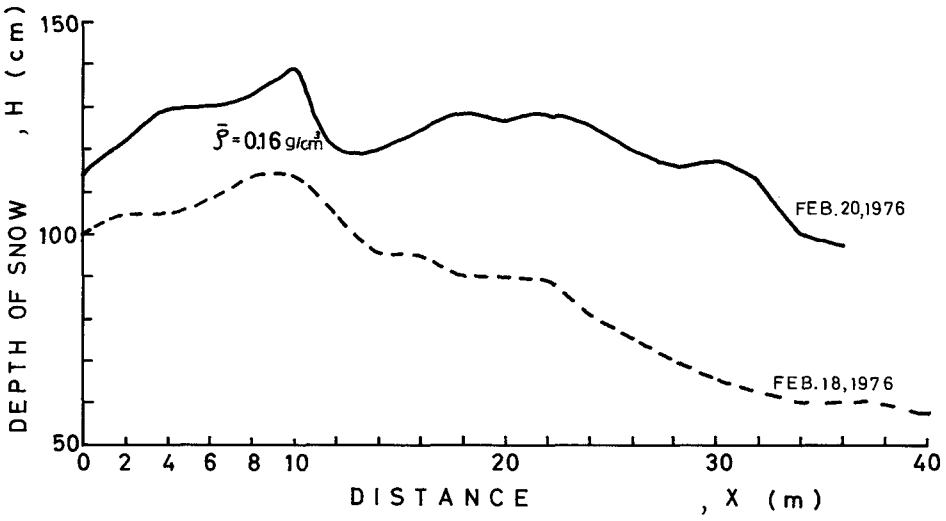

Fig. 58 Variations in depth of a snowdrift measured along leeward against the huts. Abscissa correspond to x direction shown in Fig. 57.

required solution of equation (40) is:

$$n/n' = (z/z')^{-w/kU_*} \tag{42}$$

where the prime denotes a fixed reference level. The relation between the horizontal mass flux of snow $q(z)$ at any height z and particle concentration $n(z)$ is given by:

$$n(z) = q(z)/u(z), \tag{43}$$

where $u(z)$ is the wind speed at the height z.

Representative examples of drift density are shown in Figure 59. It is seen in Figure 59 (c) that the drift density profile obtained at the site marked by n_{rf} roughly fits equation (42) of turbulent diffusion, whereas other profiles do not fit the equation. Now, we will consider a mechanism of deposition or erosion. Let drift density ratios be defined by $(n_d - n_{rf})/n_{rf}$ and $(n_e - n_{rf})n_{rf}$, than inequalities (44) and (45) correspond to deposition and erosion, respectively; i.e.,

$$(n_d - n_{rf})/n_{rf} > 0 \tag{44}$$

$$(n_e - n_{rf})/n_{rf} < 0 \tag{45}$$

If the inequalities are formed, then inequalities (44) and (45) mean the states of saturation and unsaturation by turbulent diffusion in the air, respectively. Thus, Figure 60 gives plots of drift density ratio versus height obtained from data shown in Figure 59 (c). As shown in Figure 60, the relations of the inequalities were formed at the height less than 30 cm above the surface

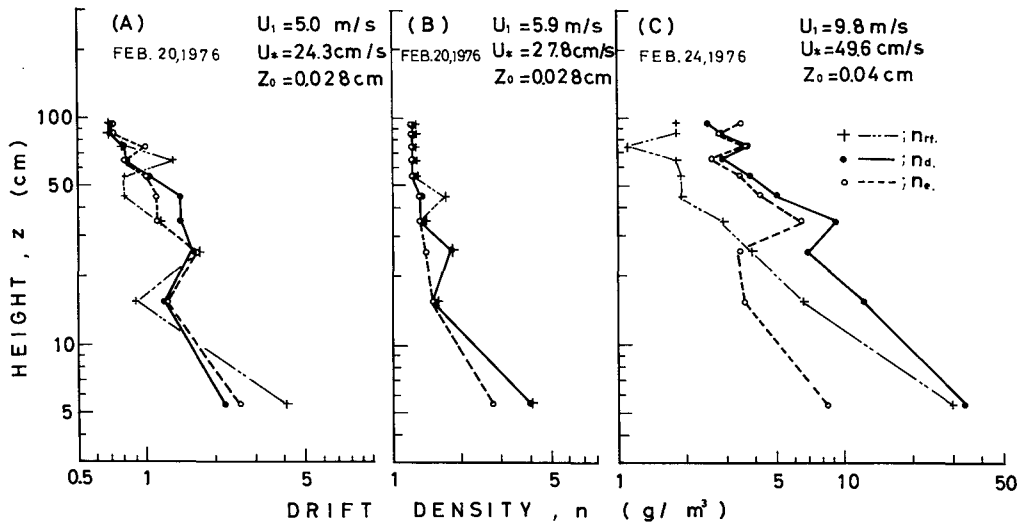

Fig. 59 Profiles of snow drift density obtained around an obstruction.

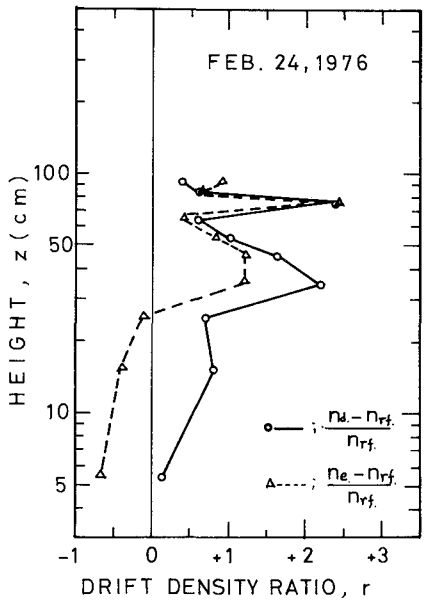

Fig. 60 Profiles of drift density ratio denoted by equations (44) and (45). Data obtained on Feb. 24, 1976, are shown in Fig. 59.

when the wind speed at the height of 1 m was about 10 m sec^{-1}. It is meant by the above fact that an excesive amount of snow particles that come into the air at lower heights will be deposited onto the surface. In general, snow particles are preferentially deposited at places where the wind speed decreases, because the snow carrying ability of the wind decreases. Such changes in wind speed respond to changes in slope.

BALL (1960) proposed that the speed of a uniform flow on the ice slope of Antarctica is given by:

$$V^3 = \frac{Q_0 \alpha g^*}{k_0}, \qquad (46)$$

where Q_0 is the rate of volume flow directly down the lines of the greatest slope, α is the surface slope, g^* is the modified gravitational acceleration given by $g^* = \theta' g/\theta$, where θ is the temperature and θ' the inversion strength, and k_0 is the friction constant given by $\rho k_0 V$.

If we know surface slopes of the ice sheet in detail, then we can estimate the wind speed by equation (46), whereby the snow drift transport can be calculated. Thus, considering a stream of wind from the interior of the ice sheet to the coast, the variation in snow accumulation may be expected to follow the variation in slope. BUDD (1966) and WHILLANS (1975) tried the above estimation over the Wilkes ice cap and an area from a traverse route to the northeast of Byrd Station in Antarctica, respectively.

Daiji KOBAYASHI (1972) measured a drift transport using box-type collectors at depositional and eroded regions, whereby he concluded that the drift transport at the former was much larger than at the latter. S. KOBAYASHI (1978) made measurements of snow drift transport on a typical snow surface which seemed to be eroded, as well as, on a small snow dune formed by an obstruction like a sled, whereby he showed that the snow drift transport measured on the latter in process of growing was three times that on the former.

Ⅶ. 3. *Wind turbulence around an obstruction*

Turbulent fluctuations in the horizontal wind speed component were measured using two sonic anemometers under a snow drifting condition around a snowdrift, the so-called "wind scoop" described in the above described in Ⅶ. 2. A plan of wind scoop around two small huts

and locations of the sonic anemometers and shown in Figure 57. The locations are marked by numbers 1-4 in the figure. Numbers 1 and 2 are on the windward and the leeward of the huts respectively. Number 3 is on the snowdrift (outside the wind scoop) and number 4 is inside of it. These location numbers correspond to the run numbers. Examples of wind fluctuations measured at numbers 3 and 4 are shown in Figure 61. The figure showed that a turbulence was larger inside the wind scoop than without it. The turbulent quantities obtained are summarized in Table 6. Runs 1 and 2 are simultaneously measured; so are runs 3 and 4. Data from the sonic anemometers were analysed as to the autocorrelation coefficients and power spectra, as are shown in Figures 62 and 63, respectively. The scale of turbulence and its characteristic times calculated from analyses of the autocorrelation coefficients are shown in Table 6. In an inertial subrange, an autocorrelation function may be experessed by equation (22) described in VI. 3. As from Table 6 the power of exponent was 0.78 outside the wind scoop, while it was 0.57 inside it. In general, the exponent was nearly equal to 2/3 in equation (22) which expresses isotropic turbulence.

The intensity of turbulence was larger within the wind scoop than without it, the former ranging from 47.8 to 25.8% and the latter from 17.4 to 18.8%. However, the scale of turbulence was of the same order except on the snowdrift (Number 3). On the snowdrift shown by location 3 in Figure 57, the scale of turbulence was 110 m; i.e., it was two times the scale in

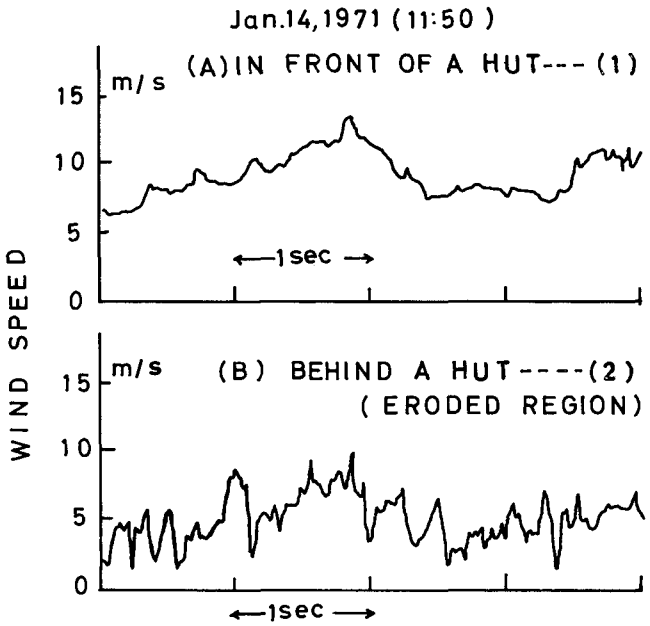

Fig. 61 Examples of longitudinal wind fluctuations by use of sonic anemometers simulaneously measured at locations (1) and (2) in Fig. 57.

Table 6. Summary of turbulent measurement around obstruction (Jan. 14, 1971)

Run	Time	T^* (sec)	Δt (sec)	z (cm)	U (m/s)	σ_u (m/s)	G (%)	T_0 (sec)	L (m)	m
1	11 : 20 ~ 11 : 26	360	1.111	145	9.1	1.7	18.8	6.2	56.4	0.78
2	〃	360	1.111	130	6.7	1.7	25.8	7.0	46.9	0.52
3	11 : 45 ~ 11 : 50	300	1.111	100	9.3	1.6	17.4	12.0	111.6	0.78
4	〃	300	1.111	100	4.2	2.0	47.8	15.0	63.0	0.62

T^* : averaging time, Δt : sampling time, Z : height of sonic anemometer, U : mean wind speed at Z, σ_u : turbulent velocity ($=\sqrt{\overline{u^2}}$), G : intensity of turbulence ($=(\sigma_u/U)\times 100\%$), T_0 : chracteristic time, L : scale of tubulenece ($=T_0 \times U$), m : power exponent of lag time in Eq. $1\text{-}R(t)=(t/T_0)^m$.

other places shown by locations 1, 2 and 4 in Figure 57. The value of 110 m may correspond to the expanding of the snow-drift on the leeward of the obstruction.

In the wind scoop, the fluctuating wind speed perpendicular to the main air stream is large, so snow particles drifting in the air are carried back into the main air stream. Accordingly, the main air stream tends to become oversaturated, as snow particles are supplied from the air in the scoop area. This oversaturated streams forms a drift at location 3, resulting in a predominant accumulation. The above results obtained from observations of turbulence support the results of drift density around the obstruction shown in Figure. 60.

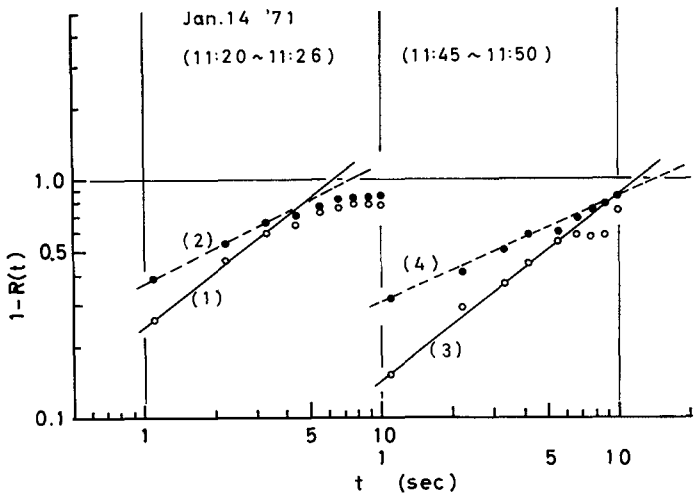

Fig. 62 Autocorrelation coefficients of longitudinal wind speed against time lag measured around the obstruction shown in Fig. 57.

In addition, the power spectra of u-fluctuation shown in Figure 63 indicate an interesting depression peak on run 3. The frequency of this peak was 0.17 Hz and corresponded to the wavelength of 54.7 m that nearly equals the scale of turbulence in the windward undisturbed by the obstruction. This fact shows that snow particles moving in the same turbulent field in the windward were deposited at parts of the snowdrift in location 3. On the other hand, there are no remarkable peaks on other power spectra shown in Figure 63.

The power spectrum in the inertial subrange is given by the so-called "$-\frac{5}{3}$" law expressed by equation (27). As shown in the figure, the frequency limit of the inertial subrange varies from 0.05 to 0.2 Hz.

VII. 4. *Large-scale phonomena between wind turbulence and an obstruction (example of the Yamato bare ice field)*

Recently, meteorite pieces were discovered in large numbers by Japanese Antarctic Research Expeditions near the southestern foot of the Yamato Mountains in East Antarctica. Since they were found in a bare ice area, KUSUNOKI (1975) pointed out that ablation will expose meteorites buried in the ice mass and it may contribute to the concentration of meteorites in

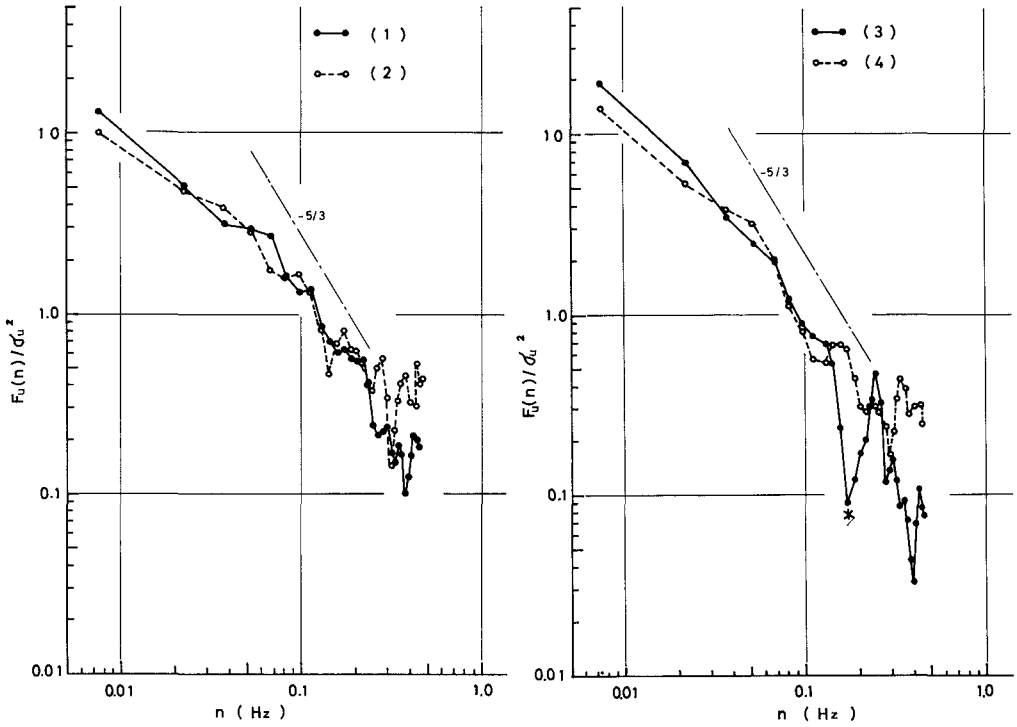

Fig. 63 Normalized power spectral densities of longitudinal component of wind fluctuations measured around the obstruction shown in Fig. 57.

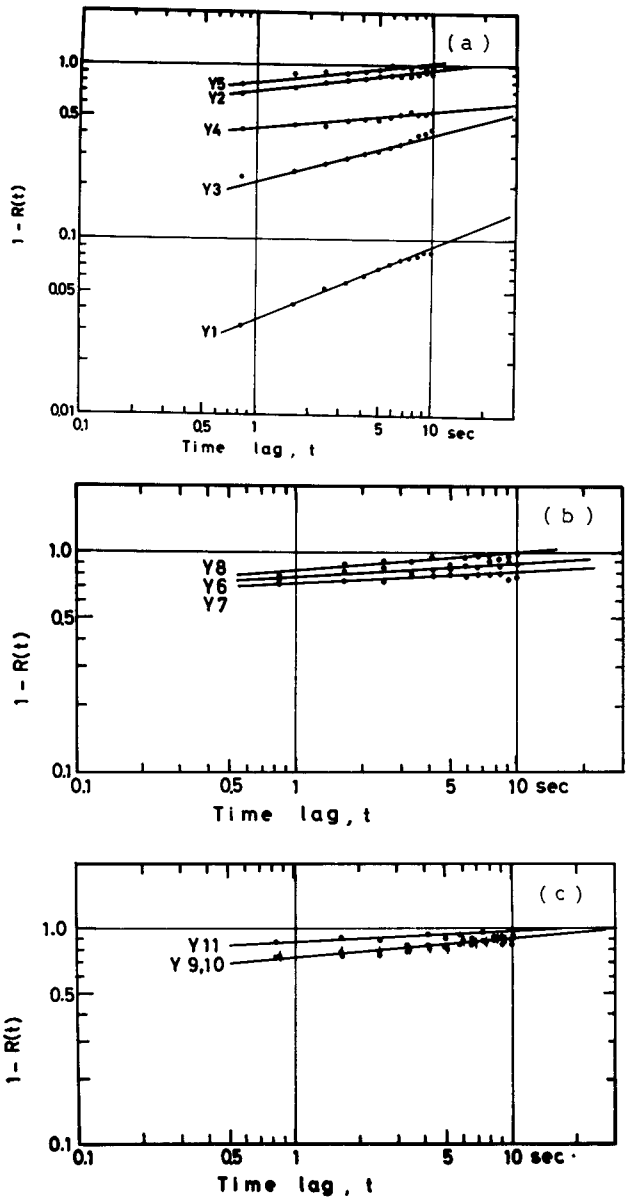

Fig. 64(a)~(c) Autocorrelation coefficients of vertical wind speed against time lag in a hydraulic jump of a katabatic wind obtained at the Yamato bare ice field.

this area. The average net ablation of 5.2 cm year^{-1} in terms of ice thickness was obtained between 1969 and 1973 in the area (YOKOYAMA , 1975). Consequently, energy and mass exchanges between the air and the ice mass must play an important role in preservation of the ice surface (KOBAYASHI , 1979).

Micrometeorological observations were carried out on a bare ice field located on the leeward of massifs E and F of the Yamato Moutains (see Figure 2 in chapter II).

For a comparison between wind turbulence around a smallscale obstruction described in the above and wind turbulence around a large-scale obstruction, observations were made of vertical wind speed fluctuations at the Yamato bare ice field which is marked by the presence of a strong hydraulic jump associated with vortexes, using a one-component ultrasonic anemometer.

Eleven examples of autocorrelation coefficients are shown in Figures 64 (a), (b) and (c). The characteristics times given in Table 7 show a wide change from 8 to 5000 sec corresponding to the scale of turbulence lying between 80 m and 50 km. Namely, there are many vortexes varying in size in the hydraulic jump. The larger vortexes may be Karman vortexes generated by the Yamato Mountains. The vortexes contribute to the expanding of the bare ice field on the leeward of the Yamato Mountains, playing an important role in preservation of the bare ice surface, which results in an energy exchange between the vortexes and the ice.

Meanwhile, Figures 65 (a), (b) and (c) show some examples of normalized power spectral densities of vertical wind speed fluctuation in a hydraulic jump in a katabatic wind obtained at the Yamato bare ice field. The magnitudes of spectral estimates have large differences among each run. As pointed out above, it is suggested that many vortexes with various sizes are

Table 7. Mean and turbulent parameters obtained at Yamato bare ice field

Run	Date 1973	Time(L.T.)	U(2.2m) m/s	U_* m/s	R_i(1.7m)	σ_w m/s	σ_w/U_*	T_w sec	m_w
Y 1	Dec.1	1400−1412	9.2	0.46	−0.005	0.71	1.54	2700	0.11
Y 2	〃	1658−1718	11.7	0.52	−0.001	0.13	0.24	15	0.13
Y 3	〃	1752−1802	11.7	0.52	−0.001	0.32	0.61	350	0.26
Y 4	〃	2037−2051	10.1	0.50	0.013	0.31	0.63	5000	0.39
Y 5	〃	2350−2403	10.1	0.50	0.013	0.14	0.28	8	0.11
Y 6	Dec.2	0530−0543	12.5	0.60	−0.006	0.19	0.32	60	0.06
Y 7	〃	0900−0916	11.6	0.65	−0.005	0.34	0.53	320	0.06
Y 8	〃	1025−1041	10.1	0.52	−0.002	0.15	0.29	11	0.08
Y 9	〃	1343−1359	10.1	0.52	−0.018	0.22	0.43	15	0.13
Y10	〃	1540−1557	10.1	0.52	−0.010	0.21	0.40	15	0.13
Y11	〃	1745−1759	10.1	0.52	0	0.34	0.66	17	0.05

U_* : Friction velocity, R_i : Gradient Richardson number, σ_w : Standard deviation of vertical vertical wind velocity, T_w : Characteristics time, m_w : Value of exponent in eq. (22).

present in the flow. We cannot identify peaks that are not associated with the hydraulic jump. In spite of the unstable conditions described in Ⅳ. 1, the slope of spectra equals roughly $n^{-\frac{2}{3}}$ over the frequency range. In general, the levels of power obtained at the Yamato bare ice field were higher than those obtained at Mizuho Station.

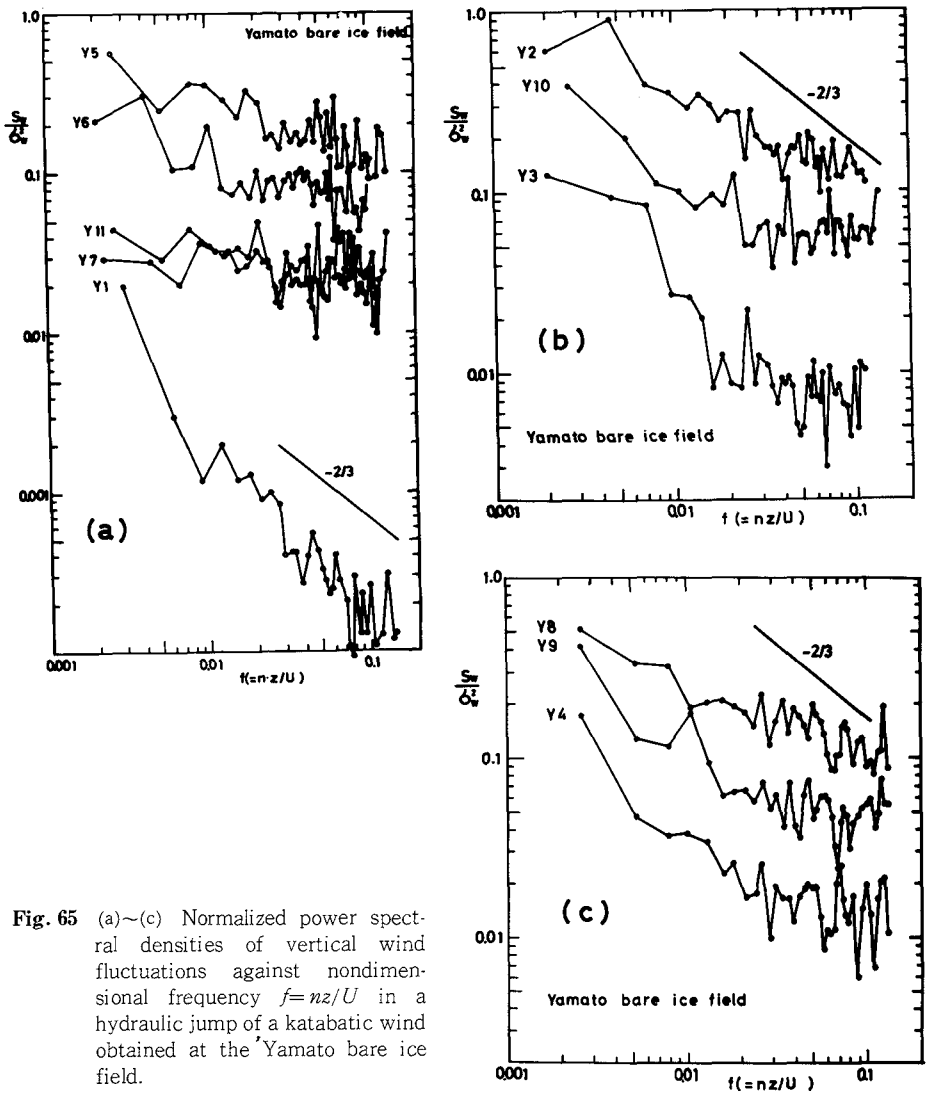

Fig. 65 (a)~(c) Normalized power spectral densities of vertical wind fluctuations against nondimensional frequency $f=nz/U$ in a hydraulic jump of a katabatic wind obtained at the Yamato bare ice field.

VIII. Discussion and concluding remarks

Considering importance of transfer phenomena in an energy exchange between the wind and the surface of dry snow or bare ice, i.e. wind-snow interaction, this paper has the main purpose of identifying characteristics of such interaction in light of a very limited knowledge about the structure of wind turbulence over the surface of snow or ice during the drifting of snow despite a great number of fundamental investigations on lessening visibility and snow drifts, which have brought about serious truble in human life, not to mention the lack of a fairly precise knowledge about turbulence in drifting snow and katabatic winds blowing over the sloped ice sheet in Antarctica.

The results of a study of some of the interactions are summarized as follows:

(1) Measurements of friction velocity against snow surfaces of various features revealed relations between threshold shear stress and surface snow density, in which the former decreases with an increase in the latter. According to definitions by KUROIWA et al. (1976) of surface irregularities of snow crystals and ice particles, dendritic crystals have larger values of irregularities than needle and columnar crystals, whereas, because of round and spherical shapes, pulverized snow partices have much smaller ones, near unity, than the foregoing crystals.

The small density of surface snow corresponds to preservation of crystal shapes of new snow, whereby the above relation is held. Also, the surface drag force and the so-called angle of repose depend on surface irregularities and mutual adhesion of particles, in a larger degree in case of the angle of repose. Pointing out that, if both irregularities and adhesion are large, the angle of repose becomes large and that the reverse is also true, KUROIWA et al. (1967) reported that the natural snow crystals observed at −35°C and pulverized snow obtained at the same temperature had the angle of repose of approximately 63 and 40 deg, respectively.

(2) The threshold shear stress described above is referred to snow particles subjected to an effect of saltation motion, so by wind-tunnel experiments of generation of drifting snow the threshold shere stress in the absence of such motion was obtained, which was 16 dyne cm^{-2} much large than 0.5 dyne cm^{-2} obtained at a field observation. This discrepancy suggests that a mechanical impingement of snow particles saltating on the surface is most important for generation of drifting snow.

(3) The values of threshold turbulent speed obtained in wind-tunnel and field measrements of generation of drifting snow were 0.7 and 0.6 m sec^{-1}, respectively.

(4) Movement of a transverse snow-wave was the same as that of a drift in terms of occurrence of deposition and erosion in an alternating sequence, in which irregulatities in deposition were influenced by the scale of wind turbulence. EXNER (1932) considered the rate of advance of sand-dune as shown in Figure 66 and showed the follwing equation:

$$C=\frac{a\cdot Q}{\rho_s\cdot h}, \tag{47}$$

where C is rate of advance (cm min^{-1}), h is wave height (cm), ρ_s is bulk density of deposited sand (g cm^{-3}) Q is sand drift rate in the air (g cm^{-1} min^{-1}) and a is efficiency of deposition. If movement of transverse snow-wave assumed the same as that of sand-dune, then we can calculate the rate of snow-wave, using the values for snow, that is, Q obtained by D. KOBAYASHI (1972), h=10 cm, ρ_s= 0.1 g cm^{-3} and a=0.5. The results showed in Figure 67. In the figure, the results for sand-dune also showed by the dashed line, which was measured by NAKANO (1969).

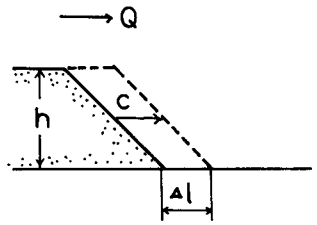

Fig. 66 Schematic representation of snow-wave travel.

(5) when a transverse snow-wave was being formed, the wind shear near the snow surface

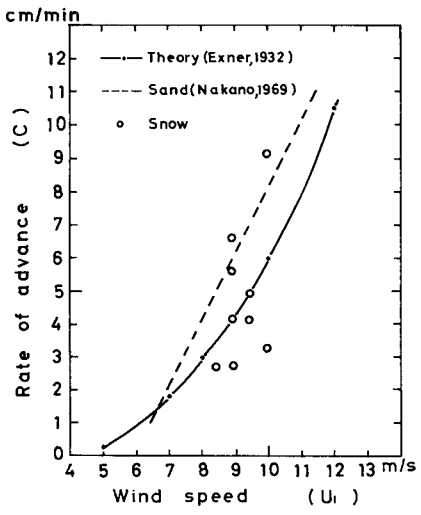

Fig. 67 Relation between rate of advance of snow-wave and wind speed at height of 1 m. Open circles represent snow-waves and solid line calculated by eq. (47) are in accord with the data. Dashed line represents rate of advance of sand-dune (NAKANO, 1969).

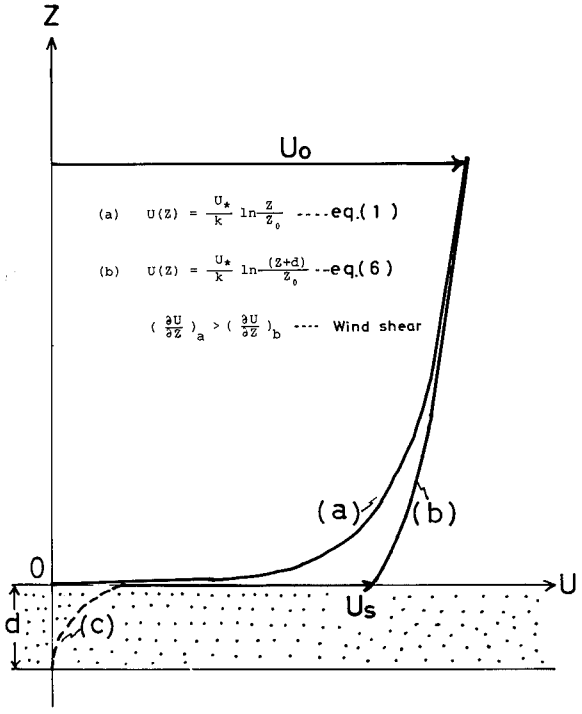

Fig. 68 Schematic representation of wind speed profiles above the snow surface for comparison between two equations (1) and (6). U_s means a surface wind speed calculated from equation (6) at z=0. In this case wind sear is smaller than of equation (1).

was weakened, as shown in Figure 68. The momentum transfer is seen having a spectral peak corresponding to the wavelength of the snow-wave, which shows that the upward direction is dominant and that the feed back of the downward momentum transfer causes the snow-wave to grow upward due to weakening of the wind shear near the snow surface.

The wavelength of the transverse snow-wave was nearly of the same order of magnitude as the scale of wind turbulence. One of the most interesting aspects of this phenomenon is its similarity to the wavelike cloud in the atmosphere and the wind wave in the ocean. A theoretical treatment of snow-waves has not been made to date despite a large literature on wind-waves and extensive theoretical work on flows over sand waves (e.g., TAYLOR and DYER, 1977; KENDALL, 1970).

(6) As for the scale of wind turbulence calculated from characteristics times, it was smaller in drifting snow than in nondrifting snow. It was in agreement with the scale of patterns marked by erosion on the snow surface; it varied inversely with the mean wind speed at the height of 1 m, transverse snow-waves disappearing, when it was 15 m sec^{-1} and above whereupon longitudinal patterns will become dominant with increaseing scale of wind turbulence.

(7) Observations of snow drift formation around an obstruction which constitutes one of subjects of the wind-snow interaction, were made concerning turbulent fluctuations in wind speed and vertical distribution of snow drift density.

Concentration of snow particles in the air in such a degree that they were supersaturated was indispensable for particles of drifting snow to deposit on the surface. In this connection, D. KOBAYASHI (1972) reported of a relation between the degree of saturation of a snowdrift and the mean length of saltation paths of snow particles concerning erosion and deposition.

Acknowledgements

The author wishes to express his thanks to Drs. T. ISHIDA, K. KOJIMA, G. WAKAHAMA, S. KINOSITA, N. MAENO and D. KOBAYASHI of the Institute of Low Temprerature Scicence, Hokkaido University, for their helpful discussions and encouragement throughout the study. He also is grateful to Drs. K. KUSUNOKI and R. HIRASAWA of the National Institue of Polar Research, and Dr. R. NARUSE and all the members of the wintering party of the 14th Japanese Antarctic Research Expedition for their helpful assistance in Antractica. The author is indebeted to Mr. H. NARITA, Dr. N. ISHIKAWA, Ms. Y. UEMATSU and Ms. S. NAGAYAMA for their assistance in preparing the manuscript. Finally, he also sincerely thanks Prof. C. MAGONO of Hokkaido Unisersity for his kind and useful suggestions.

Statistical calculations given in this paper were computed by aid of an electronic computer, FACOM 230-75, of Hokkaido University Computing Center.

References

AGETA, Y. 1971 Some aspects of the weather condition in the vicinity of the Mizuho Plateau, East Antarctica.
Antarctic Rec., **41,** 42-61 (in Japanese).

ASAI, T. 1970 Three-dimensional features of thermal convection in a plane Couette flow. *J. Meteorol. Soc. Japan,* **48,** 18-29.

ASHIDA, K. and TANAKA, Y. 1967 Experimental study on sand waves. Disaster Prevention Res. Inst. Ann. Kyoto Univ. **10,** 121-132(in Japanese).

AXFORD, D.N. 1971 Spectral analysis of an aircraft observation of gravity waves. *Quart. J. Roy. Meteorol. Soc.,* **97,** 313-321.

BAGNOLD, R.A. 1954 The Rhysics of Blown Sand and Desert Dunes. Methuen, London, 265pp.

BALL, F.K. 1960 Winds on the ice slopes of Antarctica. Antarctic Meteorology, Oxford, Pergamon Press, 9-16.

BATCHELOR, G.K. 1953 The Theory of Homogeneous Turbulence. Cambridge University Press, 197 pp.

BLACKMAN, R.B. and TUKEY, J.W. 1958 The Measurement of Power Spectra. Dover Publications, Inc., New York, 190pp.

BUDD, W. 1966 Glaciological studies in the region of Wilkes, Eastern Antarctica, 1961. *ANARE Sci. Rep., Ser. A,* **88,** 1-149.

BUDD, W., DINGLE, R. and RADOK, U. 1966 The Byrd snow drift project; outline and basic results. *Antarctic Res. Ser.,* **9,** 71-134.

BUSINGER, J.A. 1965 Eddy diffusion and setting speed in blown snow. *J. Geophy. Res.,* **70,** 3307-3313.

CAUGHEY, S.J. and REACINGS, C.J. 1975 An observation of waves and turbulence in the earth's boundary layer. *Boundary-layer Meteorol.,* **9,** 279-296.

CAUGHEY, S.J. 1977 Boundary-layer turbulence in stable conditions. *Boundary-Layer Meteocol.,* **11,** 3-14.

CORNISH, V. 1914 Waves of Sand and Snow. T. Fisher Unwin, London, 383pp.

DALRYMPLE, P.C. 1966 A physical climatology of the Antarctic Plateau. *Antarctic Res. Ser.* **9** (AGU) 195-231.

DOUMANI, G.A. 1966 Surface structures in snow. *In* Physics of Snow and Ice, Part 2 (H, Ôura, *ed.*) Inst. Low Temp. Sci., Sapporo, 1119-1136.

DYUNIN, A.K. 1963 Solid flux of snow-bearing air flow. *Natl Res. Council., Canada, Techn. Trans.,* **1102,** 25pp.

EXNER, F.M. 1932 Zur Dynamik der Bewegunsformen auf des Erdoberfläche gerl. *Beitr. z. Geophysik Supl. Bd.* **1.**

FUKUOKA, S. 1968 Generation, development and spectrum of sand-waves. *Dep. Civil Eng., Tokyo Inst. Tech. Rept.* **4,** 45-55.

GAMO, M. and YOKOYAMA, O. 1957 Observed characteristics of the standard deviation of the vertical wind velocity in upper part of the atmospheric boundary layer. *J. Meteoro. Soc. Japan,* **53**, 412-424.

HATAKEYAMA, H. 1963 Snow cover and wind. *Applied Phys.,* **5**, 588-592 (in Japanese)

HIRO, M. 1968 Equilibrium-range spectra of sand waves formed by flowing water. *J. Fluid Mech.,* **34**, 565-573.

HOLMGREN, B. 1971 Climate and energy exchange on a sub-polar ice cap in summer. Part c; On the katabatic winds over the north-west slope of the ice cap, variations of the surface roughness. Arctic Institute of North America Devon Island Expedition 1961-1963, Meteorogiska Institutionen Uppsala Universitet, Medclelande Nr 109.

INOUE, E. 1952 On the structure of wind near the ground, *Bull. Natl Inst. Agric. Sci. Ser.* **A2**, 1-9 (in Japanese).

INOUE, M. and FUJINO, K. 1977 Measurements of drifting snow at Mizuho Camp, 1974-1975. *Antarctic Rec.*, **60**, 1-12.

JACKSON, B.S. and CARROLL, J.J. 1978 Aerodynamic roughness as a function of wind direction over asymmetric surface elements. *Boundary-Layer Meteorol.*, **14**, 323-330.

KAIMAL, J.C. 1973 Turbulence spectra, length scales and structure paramenter in the stable surface layer. *Boundary-Layer Meteorol.*, **4**, 289-309.

KAWAMURA, R. 1951 Study of sand movement by wind. *Rept. Techn. Res. Inst., Tokyo Univ.*, **5**, 95-112 (in Japanese).

KENDALL, J.M. 1970 The turbulent boundary layer over a wall with progressive surface waves. *J. Fluid Mech.*, **41**, 259-281.

KIKUCHI, T. and ISHDA, T. 1976 A note on the increase of roughness during drifting snow. *Low Temp. Sci., Ser. A*, **34**, 87-91 (in Japanese).

KINOSITA, S. and WAKAHAMA, G. 1960 Thin sections of deposited snow made by the use of aniline. *Contributions from Inst Low Temp. Sci.*, **15**, 35-45.

KOBAYASHI, D. 1972 Studies of snow transport in low-level driftiong snow. *Contributions from Inst. Low Temp. Sci. Ser. A*, **24**, 1-58.

KOBAYASHI, S. 1971 Development and movement of wavy features on the snow surface during snow drifting. *Low Temp. Sci., Ser. A*, **29**, 81-94 (in Japanese with English summary).

KOBAYASHI, S. and YOKOYAMA, K. 1976 Observations of the stationary katabatic winds in Mizuho Platau, East Antarctica. *Ant. Rec.*, **56**, 1-13.

KOBAYASHI, S. and YOKOYAMA, K. 1977 Measurements of drifting snow on the route between Syowa Station and Mizuho Camp, 1973. *JARE Date Rep.*, **36**, 154-155.

KOBAYASHI, S. 1978a Vertical structure of katabatic winds in Mizuho Plateau. *Mem. Natl Inst. Polar Res., Spec. Issue*, **7**, 72-80.

KOBAYASHI, S. 1978b Snow transport by katabatic winds in Mizuho Camp area, East Antarctica. *J. Meterol. Soc. Japan*, **56**, 130-139.

KOBAYASHI, S. 1979 Snow features of the turbulent transfer on the bare ice field near the Yamato Mountains, East Antarctica. *Mem. Natl Inst. Polar Res., Spece. Issue*, **11**, 9-18.

KUROIWA, D., MIZUNO, Y. and TAKEUCHI, M. 1967 Micromeritical properties of snow. *In* Physics of Snow and Ice, Part 2 (Ôura, *ed.*), Inst. Low Temp. Sci., Sapporo, 751-772.

KUROIWA, D. 1975 Mechanics and structure of snow as a dispersed system. Proceeding of the International Symposium on Snow Mechanics, Grindelwald, 1974. The International Association of Hydrological Science, Publication No. 114, 3-15.

KUSUNOKI, K. 1975 A note on the Yamato meteorites collected in December 1969. *Mem. Natl Inst. Polar Res., Spec. Issue*, **5**, 1-8.

LILJEQUIST, G.H. 1957 Energy exchange of an Antarctic snowfield. Part 1c : Wind structure in the low layer. Norwegian-British-Swedish Antarctic Expedition, 1949-52. Scientific Res., II.

LOEWE, F. 1956 Etudes de glaciogie en Terre Adelie, 1951-1952. Pario : Hermann.

MAENO, N. and NISHIMURA, K. 1978 Studies of fluidized snow I, Formation of fluidized snow and its general property. *Low Temp. Sci., Ser. A* **36**, 77-92 (in Japanese with English summary).

MAENO, N. and NISHIMURA, K. 1979 Fluidization of snow. *Cold Regions Sci. and Tech.*, **1**, No.2, 109-120.

MAL, S. 1930 Forms of stratitied clouds. *Beitr. Phys. Atomos.*, **17**, 40-68.

MAKI, T. 1974 Turbulence characteristics and micrometeorological structure of atmospheric surface layer in stable stratification in Antarctica. *Mem. Natl Inst. Polar Res. Ser. B*, **2**, 1-65.

MASCART, P., ISAKA, H. and GUILLEMET, B. 1978 Kelvin-Helmholtz waves observed by aircraft at different stages of their life-cycle in a low-level inversion. *Boundary-layer Meteorol.*, **15**,

31-55.

MELLOR, M. and RADOK, U. 1960 Some properties of drifting snow. in Antarctic meteorology, Oxford, Porgamon Press, 333-346.

MELLOR, M. 1965 Blowing snow. Cold Regions Science and Engineering, Part III, Section A3C, CRREL, Hanover, 1-79.

MELLOR, M. 1970 A brief review of snowdrifting research. *In* snow Removal and Ice Control Research *Highway Res. Board, Spec. Rept.,* **115**, 196-209.

MONIN, A.S. and YAGOLOM, A.M. 1971 Statistical Fluid Mechanics. Vol. 1, Cambridge, the MIT Press, 769pp.

NAKANO, T. 1969 The plain in Japan. Kokin Shoin, 320pp., (in Japanese)

NARITA, H. 1978 Controlling factors of drifting snow *Mem. Natl Inst. Polar Res., Spec. Issue,* **7**, 81-92.

NARUSE, R. 1970 Measurement of drifting snow on the coastal region of Antarctica, near Syowa Station. *Low Temp. Sci., Ser. A,* **28**, 147-154 (in Japanese).

NORDIN, C.F. and ALGERT, J.H. 1966 Spectral analysis of sand waves. *J. Hydraulisc Division, ASCE 92, No. HY5,* 95-114.

ÔURA, H. 1966 Studies of blowing snow I. *In* Physics of Snow and Ice, Part 2 (H. Ôura, *ed.*), Inst. Low Temp. Sci., Sapporo, 1085-1097.

ÔURA, H., ISHIDA, T., KOBYASHI, D., KOBAYASHI, S. and YAMADA, T. 1967 Studies on blowing snow II. *In* Physics of Snow and Ice, Part 2 (Ôura, *ed.*), Inst. Low Temp. Sci., Sapporo, 1099-1117.

ÔURA, H. and YAMADA, T. 1966 On the orientation of snow dunes in the vicinity of Soya coast. *Ant. Rec.,* **26**, 30-40 (in Japanese).

ÔURA, H. 1968 On the study of generation of drifting snow. *Japanese Soc. Snow and Ice,* **30**, 169-175 (in Japanese).

RAYMENT, R. and CAUGHEY, S.J. 1977 An investigation of the turbulence balance equations in the atmospheric boundary layer. *Boundary-Layer Meterol.,* **11**, 15-26.

RUSIN, N.P. 1961 Meteorological and radiational regime of Antarctica. (Translated from Russion), Israel Program for Scientific Translations Jerusalem 1964.

SELIGMAN, G. 1962 Snow Structure and Ski Field. R.&R. Clark, Ltd., Edinburgh, 555pp.

SETHURAMAN, S. 1977 The observed generation and breaking of atmospheric internal gravity waves over the ocean. *Boundary-Layer Meteorol.,* **12**, 331-349.

SHIOTAI, M. and ARAI, H. 1952 A short note on the snow-storm. Second National Congress for Applied Mechanics, Science Council of Japan.

SOMMERFELD, R. and BUSINGER, J.A. 1965 The density profile of blown snow. *J. Geophy. Res.,* **70**, 3303-3306.

TAYLOR, R.A. and DYER, K.R. 1977 Theoretical models of flow near the bed and their implications for sediment transport. in the Sea, Vol.6, 579-601.

TENNEKES, H. and LUMLEY, J.L. 1972 A first course in turbulence. MIT press, 300 pp.

UNTERSTEINER, N. and BADGLEY, F.I. 1965 The roughness parameters of sea ice. *J.Geophys. Res.,* **70**, 4573-4577.

WATANABE, O. 1978 Distribution of surface features of snow cover in Mizuho Plateau. *Mem. Natl Inst. Polar Res. Special Issue,* **7**, 44-62.

WHILLANS, I.M. 1975 Effect of inversion winds on topographic detail and mass balance on inland ice sheet. *J. Glaciol.* **14**, 85-90.

YAMADA, T. 1974 Surface meteorogical condition in the region between Syowa Station and Mizuho Camp, Mizuho Plateau, East Antarctica *Antarc. Rec.,* **50**, 1-20(in Japanese).

YOKOYAMA, K. 1975 Net accumulation by stake measurements. *JARE Data Rep.,* **28** (Glaciol.), 62-82

YOKOYAMA, O. GAMO, M. and YAMAMOTO, S. 1977 On the turbulence quantities in the neutral atmospheric boundary layer. *J. Metero. Soc. Japan,* **55**, 312-318.

YOSHIDA, Z. 1977 Air flow induced in a snow cover by the wind blowing over its surface. *Low Temp. Sci., Ser. A,* **35**. 47-65(in Japanese).